Resource

Cell

Cross-Species Single-Cell Analysis Reveals Divergence of the Primate Microglia Program

Graphical Abstract

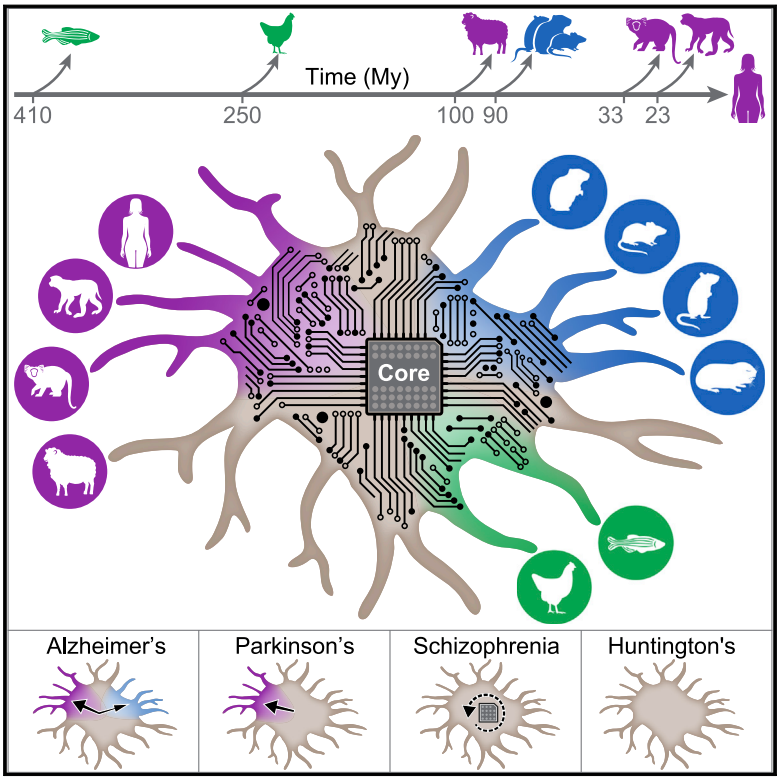

Authors

Laufey Geirsdottir, Eyal David, Hadas Keren-Shaul, ..., Daniel Erny, Ido Amit, Marco Prinz

Correspondence

daniel.erny@uniklinik-freiburg.de (D.E.), ido.amit@weizmann.ac.il (I.A.), marco.prinz@uniklinik-freiburg.de (M.P.)

In Brief

Single-cell sequencing of microglia across evolutionary timescales leads to definition of a conserved core expression program and identification of heterogeneity in human microglia lacking in other species.

Highlights

- Microglia single-cell expression and morphology across 450 million years of evolution
- Microglia express a conserved core program, including CNS ligand-receptors pairs
- Human microglia show significant heterogeneity in comparison with all mammals
- Identification of disease-associated microglia gene expression modules in humans

Geirsdottir et al., 2019, Cell *179*, 1609–1622
December 12, 2019
https://doi.org/10.1016/j.cell.2019.11.010

CellPress

Resource

Cell

Cross-Species Single-Cell Analysis Reveals Divergence of the Primate Microglia Program

Laufey Geirsdottir,[1,23] Eyal David,[1,23] Hadas Keren-Shaul,[1,2,23] Assaf Weiner,[1] Stefan Cornelius Bohlen,[3] Jana Neuber,[3] Adam Balic,[4] Amir Giladi,[1] Fadi Sheban,[1] Charles-Antoine Dutertre,[5,6] Christine Pfeifle,[7] Francesca Peri,[8] Antonella Raffo-Romero,[9] Jacopo Vizioli,[9] Kaspar Matiasek,[10] Christian Scheiwe,[11] Stephan Meckel,[12] Kerstin Mätz-Rensing,[13] Franziska van der Meer,[13] Finnbogi Rutur Thormodsson,[14] Christine Stadelmann,[15] Noga Zilkha,[16] Tali Kimchi,[16] Florent Ginhoux,[5,17,18] Igor Ulitsky,[19] Daniel Erny,[3,20,24,*] Ido Amit,[1,24,25,*] and Marco Prinz[3,21,22,24,*]

[1]Department of Immunology, Weizmann Institute of Science, Rehovot, Israel
[2]Life Science Core Facility-Israel National Center for Personalized Medicine (G-INCPM), Weizmann Institute of Science, Rehovot, Israel
[3]Institute of Neuropathology, Faculty of Medicine, University of Freiburg, Freiburg, Germany
[4]The Roslin Institute and Royal (Dick) School of Veterinary Studies, University of Edinburgh, Easter Bush, EH25 9RG, United Kingdom
[5]Singapore Immunology Network (SIgN), Agency for Science, Technology and Research (A*STAR), Singapore, Singapore
[6]Program in Emerging Infectious Disease, Duke-NUS Medical School, 8 College Road, Singapore, Singapore
[7]Department of Evolutionary Genetics, Max-Planck-Institute for Evolutionary Biology, Ploen, Germany
[8]Institute of Molecular Life Sciences, University of Zurich, Zurich, Switzerland
[9]Universite Lille, Inserm, U-1192—Laboratoire Protéomique, Réponse Inflammatoire et Spectrométrie de Masse-PRISM, Lille, France
[10]Section of Clinical & Comparative Neuropathology, Centre for Clinical Veterinary Medicine, Ludwig-Maximilians-Universität München, Munich, Germany
[11]Clinic for Neurosurgery, Faculty of Medicine, University of Freiburg, Freiburg, Germany
[12]Department of Neuroradiology, Medical Center, Faculty of Medicine, University of Freiburg, Freiburg, Germany
[13]German Primate Center, Leibniz Institute for Primate Research, Göttingen, Germany
[14]Innovation Center Iceland, Reykjavik, Iceland
[15]Institute of Neuropathology, University Medical Center Göttingen, Göttingen, Germany
[16]Department of Neurobiology, Weizmann Institute of Science, Rehovot, Israel
[17]Shanghai Institute of Immunology, Shanghai JiaoTong University School of Medicine, Shanghai, China
[18]Translational Immunology Institute, Singhealth/Duke-NUS Academic Medical Centre, the Academia, Singapore, Singapore
[19]Department of Biological Regulation, Weizmann Institute of Science, Rehovot, Israel
[20]Berta-Ottenstein-Programme, Faculty of Medicine, University of Freiburg, Freiburg, Germany
[21]Signaling Research Centres BIOSS and CIBSS, University of Freiburg, Freiburg, Germany
[22]Center for NeuroModulation, Faculty of Medicine, University of Freiburg, Freiburg, Germany
[23]These authors contributed equally
[24]These authors contributed equally
[25]Lead Contact
*Correspondence: daniel.erny@uniklinik-freiburg.de (D.E.), ido.amit@weizmann.ac.il (I.A.), marco.prinz@uniklinik-freiburg.de (M.P.)
https://doi.org/10.1016/j.cell.2019.11.010

SUMMARY

Microglia, the brain-resident immune cells, are critically involved in many physiological and pathological brain processes, including neurodegeneration. Here we characterize microglia morphology and transcriptional programs across ten species spanning more than 450 million years of evolution. We find that microglia express a conserved core gene program of orthologous genes from rodents to humans, including ligands and receptors associated with interactions between glia and neurons. In most species, microglia show a single dominant transcriptional state, whereas human microglia display significant heterogeneity. In addition, we observed notable differences in several gene modules of rodents compared with primate microglia, including complement, phagocytic, and susceptibility genes to neurodegeneration, such as Alzheimer's and Parkinson's disease. Our study provides an essential resource of conserved and divergent microglia pathways across evolution, with important implications for future development of microglia-based therapies in humans.

INTRODUCTION

Microglia are the primary resident immune cells of the CNS parenchyma and are seeded during development from mesodermal progenitors (Alliot et al., 1999; Ginhoux et al., 2010; Kierdorf et al., 2013; Gomez Perdiguero et al., 2015). Lineage tracing studies using mice have demonstrated that they can persist in the brain through local self-renewal, with no significant replenishment of monocytes during homeostatic conditions (Ajami et al., 2011; Askew et al., 2017; Hashimoto et al., 2013; Tay et al., 2018; Yona et al., 2013). They can rapidly repopulate their

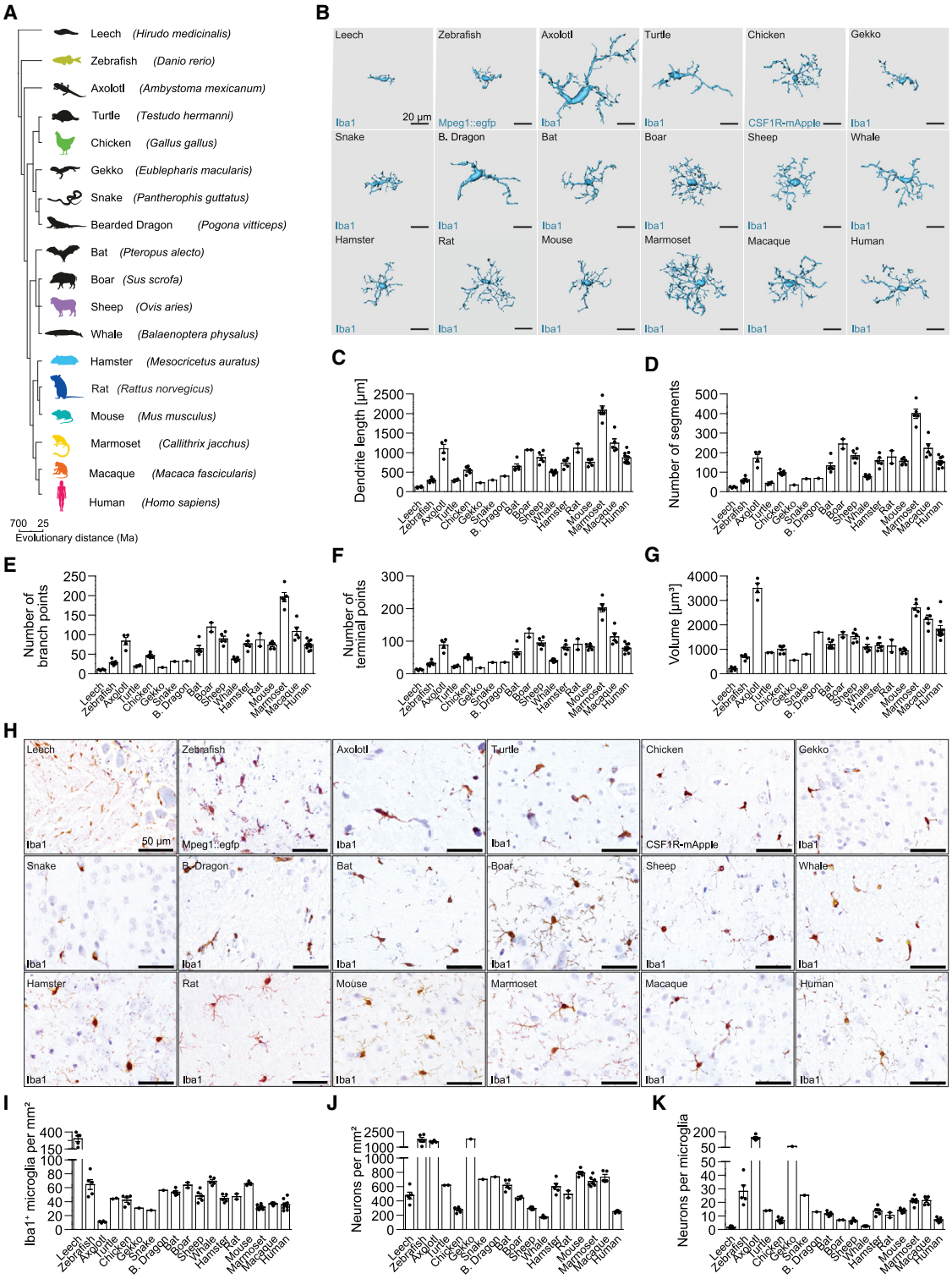

Figure 1. Quantitative Analysis of Microglia Morphology in Evolutionarily Distant Animals

(A) Phylogenetic tree based on the NCBI taxonomy of animals used in this study (generated via https://phylot.biobyte.de/). Ma, million years.

(B–G) Three-dimensional reconstruction (B; scale bars represent 20 µm) and Imaris-based automatic quantification (C–G) of the cell morphometry of cortical Iba1$^+$, Mpeg1-EGFP$^+$ (zebrafish), and CSF1R-mApple$^+$ (chicken) microglia. Each panel displays one individual sample with at least three measured cells per animal. Data are presented as mean ± SEM.

(legend continued on next page)

niche by self-renewal if depleted (Bruttger et al., 2015; Najafi et al., 2018), showing their unique adaptation to the brain parenchyma. This brain-specific tissue environment induces functional specialization of microglia, resulting in a highly distinct phenotype separate from other tissue macrophage populations (Gosselin et al., 2014; Lavin et al., 2014). Additionally, microglia have been shown to be susceptible to environmental stimuli, such as microbiome and neonatal infection (Erny et al., 2015; Thion et al., 2018).

Depending on the brain region, microglia are estimated to compose 5%–20% of all brain cells (Lawson et al., 1990; Perry, 1998). Microglia shape important brain processes, such as neuronal pruning and development (Parkhurst et al., 2013; Schafer et al., 2012). Importantly, innate immune activation is considered to be of critical pathophysiologic significance in most neurodegenerative diseases, such as Alzheimer's disease (AD), suggesting microglia as central players in disease pathology (Matcovitch-Natan et al., 2016). Recently, we and others have demonstrated that microglia-specific pathways, such as Trem2-Tyrobp and ApoE, are critical determinants in AD and other neurodegenerative diseases (Jansen et al., 2019; Lambert et al., 2013; Keren-Shaul et al., 2017). Incidences of neurodegenerative disorders have steadily increased over the last decades, in line with higher life expectancies of humans (Drew, 2018). Despite immense efforts over the past decades to find a cure for neurodegenerative disorders using transgenic animal models, large differences are observed in multiple characteristics of disease manifestation in human versus animal models. A better understanding of the conserved and divergent pathways of microglia may highlight the impact and limitation of commonly used animal models for neurodegeneration.

Large-scale sequencing of animal genomes has paved the way for characterization of genomic elements that are highly conserved across millions of years of evolution (La Manno et al., 2016; Suryamohan and Halfon, 2015). However, major challenges remain when applying this to analysis of gene expression conservation across cell types. Standard antibody-based cell type purification across species remains challenging because epitope and antibody differences and impurities of the cell population captured with these antibodies across different species significantly restrict accurate cross-species analysis (Giladi and Amit, 2018). Potentially, single-cell RNA sequencing (scRNA-seq) can overcome these challenges, bypassing the need for pure cell sorting strategies. Accordingly, scRNA-seq has been used to deconvolve immune cell type heterogeneity by identifying novel distinct immune cell subsets in health and disease (Jaitin et al., 2014; Keren-Shaul et al., 2017; Papalexi and Satija, 2018; Paul et al., 2016; Jaitin et al., 2019; Li et al., 2019) and has provided new insights into the development and evolution of cell types (La Manno et al., 2016; Pollen et al., 2015; 2014; Sebé-Pedrós et al., 2018; Treutlein et al., 2014; Zeisel et al., 2015).

Here we comprehensively characterize the conservation and divergence of the microglia program across evolution. By comparing microglia gene expression across species, we identify a conserved microglia core program in all mammals. Single-cell analysis showed that most mammalian microglia display one primary transcriptional state without any other apparent subtypes. However, predominantly in humans, we observed substantial microglial heterogeneity, with subtypes of microglia transcriptional signatures that are common to all individuals examined. Importantly, microglia also contained species- and clade-specific gene expression pathways associated with the complement system, phagocytosis, and metabolic pathways. By cross-comparing microglia gene expression with genome-wide association studies (GWASs) of human neurodegenerative diseases, we observed significant expression changes of susceptibility genes for AD and Parkinson's disease (PD) in primates and humans compared with rodents. In summary, we show the importance of cross-evolutionary comparison to better characterize human-specific microglia pathways and the relevance of these to human disease. All data generated can be visualized using an interactive web-based tool (https://amitlab.shinyapps.io/Orthologous_viewer/). In summary, our data offer an essential resource for the neuroimmunology community to move toward the development of immunotherapy-based treatments for neurodegenerative and neurodevelopmental disorders.

RESULTS

Parenchymal Microglia Display a Conserved Morphological Pattern across Evolution

To determine microglia conservation across evolution, we collected brain tissue of 18 evolutionarily distant species for detailed microscopical analysis (Figure 1A). We identified microglia using ionized calcium binding adaptor molecule 1 (Iba1), a prototypical marker for microglia, perivascular macrophages, and monocytes of humans, rats, and, mice (Prinz and Priller, 2014) that has been traditionally used to identify microglia within the parenchyma because other glial cells and neurons do not express it. Iba1 immunohistochemistry-based 3D-Imaris analysis revealed that 16 of the 18 animals were positive for parenchymal Iba$^+$ cells whereas chicken and zebrafish were not (Figure 1B). The pan-myeloid markers mPEG1 (mPEG1-GFP zebrafish) (Ellett et al., 2011) and CSF1R (CSF1R-mApple chickens) (Balic et al., 2014) were subsequently used for myeloid identification within the parenchyma of these species (Figure 1B). Microscopic analysis of Iba1$^+$, mPEG1$^+$, and CSF1R$^+$ parenchymal myeloid cells showed cells with dendritic morphology, including spindle-shaped somata and a distinct arborization pattern, as described

(H) Brain tissue was subjected to immunohistochemistry for Iba1 or stained with antibodies against the respective fluorescent proteins (zebrafish and chicken) to detect microglia. Scale bars represent 50 μm. Representative images are displayed.
(I) Number of ramified parenchymal microglia in the CNS.
(J) Number of cresyl violet$^+$ cortical neurons in the CNS.
(K) Calculated ratio of neurons per microglia.
For (H)–(K), each symbol displays one individual sample. Three to four sections per sample were analyzed. Data are presented as mean ± SEM.

before (Sierra et al., 2016; Figures 1B and S1A). The distinctive morphology and widespread distribution of these cells were highly consistent with the classical descriptions of ramified microglia. These findings suggest that CNS parenchymal cells with microglia-like morphological features and markers can be found across all of these animals, although we observed a considerable range of ramifications and cell size between species (Figures 1B and S1A). Analysis of mouse and human microglial morphology revealed a partial region-specific heterogeneity in both species, including smaller dendrite length, a smaller number of segments, and fewer branchpoints and terminal points in the molecular layer of the cerebellum (Figures S1B and S1C). In general, the overall morphology of human microglia showed the highest similarity to macaque, mouse, rat, hamster, sheep, boar, bat, and chicken microglia in terms of dendrite length, number of branching segments, terminal points, and volume (Figures 1B–1G and S1A). The highest microglial density was detected in leech ganglia with 299.0 ± 41.4 Iba1$^+$ microglia/mm^2 and lowest microglial numbers in axolotls (11.1 ± 0.7/mm^2) (Figures 1H–1I).

We quantified the number of neurons in the cortex (Figure 1J) and neurons per microglia (Figure 1K). In a correlation analysis, we detected positive correlation of microglial density per mm^2 and microglia process length across species (Figure S1D), whereas we did not observe any detectable correlation between microglial and neuronal density (Figure S1E) or microglia/neuron ratio and microglia process length (Figure S1F). In line with a previous report (Menassa and Gomez-Nicola, 2018), we detected a higher microglial density in the frontal cortex of mice (65.8 ± 1.09 cells/mm^2) compared with the human frontal cortex (35.5 ± 2.48 cells/mm^2) and more microglia in the human cerebellum (molecular layer), hippocampus, and white matter compared with the respective regions in mice (Figures S1G–S1J). In summary, histological analysis shows that microglial density varies markedly across species, even among rodents and larger mammals. Further, although microglia display similar dendritic morphology, the degree of ramification and cell size differs considerably in many of the species examined.

Characterization of the Microglia Gene Expression Program across Species

To better understand the divergence and conservation of microglia gene expression across evolution, we collected brains from three to six individuals for the eight species that had a high-quality reference genome: human, macaque, marmoset, sheep, mouse, hamster, chicken, and zebrafish. Because even carefully sorted samples for bulk RNA-seq contain contaminating cells, and scRNA-seq may potentially not be sensitive enough for detection of lowly expressed genes, we used a combined single-cell and bulk RNA-seq strategy to characterize the microglia gene program across evolution (Figure 2A; STAR Methods). Analysis of the single-cell data was then used to deconvolute the bulk RNA-seq data and remove contaminating genes (Figure 2A; STAR Methods; Baron et al., 2016).

To preserve the *in situ* transcriptional state of microglia, all samples were freshly processed and sorted by fluorescence-activated cell sorting (FACS) using a highly conserved pan immune marker: protein tyrosine phosphatase, receptor type C (Ptprc/CD45; Figure S2A; Holmes, 2006; Nagata et al., 2002; Okumura et al., 1996). Cells were sorted for massively parallel scRNA sequencing (MARS-seq2.0) analysis (Jaitin et al., 2014; Keren-Shaul et al., 2019) or for bulk RNA sequencing (Figure 2A). We collected a total of 4,458 quality-controlled (QC)-positive microglia cells from eight species as well as three to six bulk RNA-seq samples for each species (Figure S2B–S2D; Table S1). The metacell algorithm (Baran et al., 2018; Giladi et al., 2018) was used to identify homogeneous and robust groups of cells (metacells; STAR Methods). The majority of immune cells in the examined species were identified as microglia based on their gene signature. Nonetheless, most species contained some metacells that were identified as contaminating cells (Table S1). For example, in chicken, analysis of CD45$^+$ brain cells revealed two major groups of immune populations (Figure 2B). The first group expressed the microglia gene signature, including multiple typical microglia markers that have already been identified in human and mouse microglia (e.g., *SALL1*, *P2RY12*, *C1QB*; Figure 2B), whereas the second group expressed marker genes associated with T cells (e.g., *CD3E*, *RORA*, and *IL7R*) (Figure 2B). In order to focus on the microglia cells, after identification of contaminating cell clusters, we removed the genes associated with these clusters from the bulk RNA-seq data (Figure 2C, 2D, and S2E; STAR Methods). We applied this method of microglia single-cell characterization and bulk RNA-seq deconvolution data analysis to all species. Together, these findings highlight the potential of scRNA-seq to define, with minimal biases, conserved cell type transcriptional signatures across species, enabling marker-free molecular comparison of the microglia program across evolution.

Microglia Express a Core Gene Program across Evolutionarily Distant Species

To compare gene expression across species, we first defined a set of homologous genes across species. We used a "metagene" strategy to solve the one-to-many and many-to-many relationships of orthologs that have changed in evolution through duplication/deletion events (STAR Methods). Ortholog conjecture is widely accepted as a method to pair genes over evolution because orthologs diverge slowly, most explicitly in a tissue-specific manner, whereas paralogs do not (Kryuchkova-Mostacci and Robinson-Rechavi, 2016). After filtering for lowly expressed genes, we identified 8,890 genes that were expressed in microglia of at least one of the species (STAR Methods). Gene quantile normalization, followed by clustering analysis of the deconvoluted bulk and scRNA-seq of microglia across evolution, identified 17 prominent gene clusters (Figures 3A and S3A; Table S2; STAR Methods). These clusters include a microglia core signature expressed in all species (clusters 1–10), but to a lesser extent in the zebrafish and chicken, as well as clade and species-specific programs (clusters 11–17; Figures 3A and S3A). Hierarchical clustering across samples grouped the species based on their evolutionary distance and displayed two major groups, with the zebrafish and chicken microglia forming an outgroup from the mammals (Figures 3A and S3). This was not affected by the number of clusters or analysis method, and similar results were observed when applying principal-component analysis (PCA; Figure S3B). We thus removed zebrafish and chicken from further analysis to focus on the more subtle

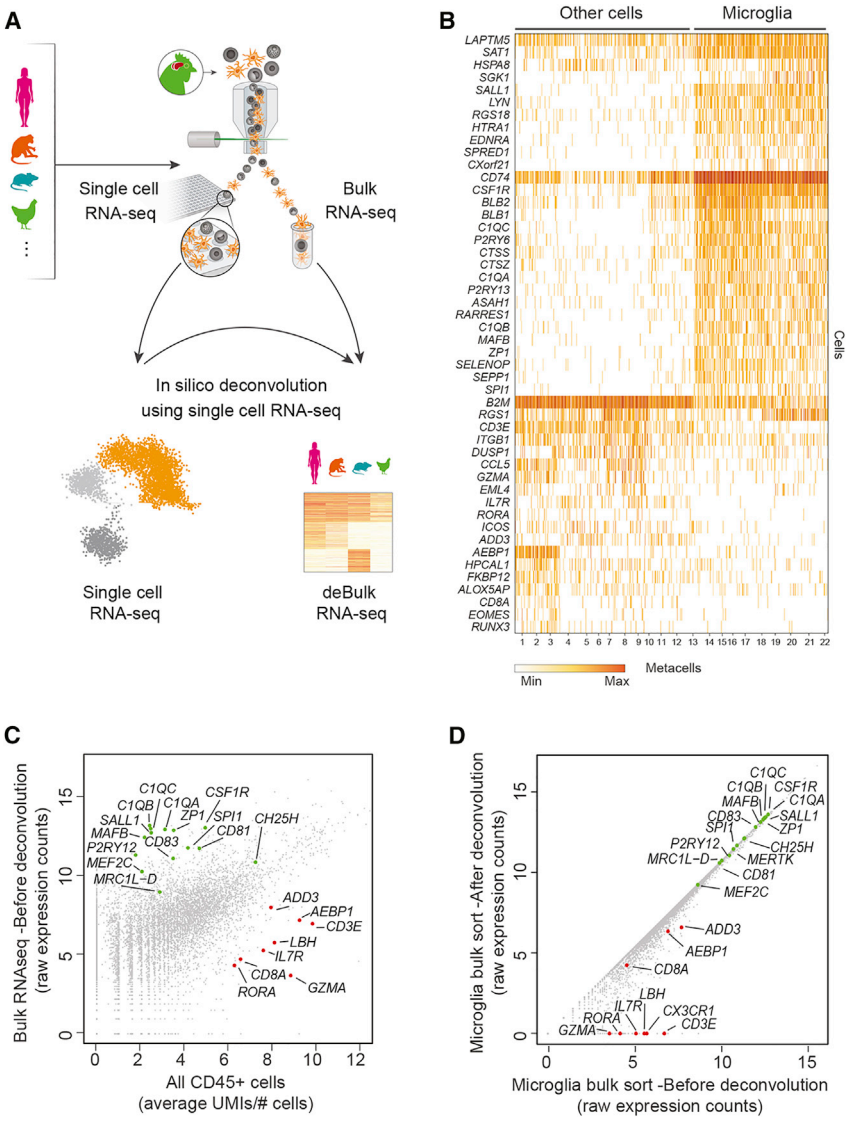

Figure 2. Transcriptional Characterization of Microglia across Species

(A) Illustrative representation of the RNA-seq strategy and cross-species characterization of microglia using flow cytometry for single-cell sorting and bulk sorting. Some of the examined species are shown as an example. deBulk RNA-seq, deconvulted bulk RNA-seq.

(B) Metacell analysis (of 629 cells and 22 metacells) and heatmap representation of 30 differentially expressed genes and marker genes from CD45$^+$ scRNA-seq-sorted cells from a chicken brain.

(C) Scatterplot (xy) showing the relationship of expressed genes between all CD45$^+$ genes from combined scRNA-seq from chicken (x) and bulk RNA-seq before *in silico* deconvolution (y).

(D) Scatterplot (xy) showing the relationship of expressed genes between bulk RNA-seq of chicken microglia before deconvolution (x) and bulk RNA-seq of chicken microglia after deconvolution (y).

changes in mammalian microglia. Macaque showed the highest similarity in expression patterns to human microglia, whereas laboratory mouse strains clustered together with wild mice and hamster (Figures 3A and S3A–S3E; Table S3; STAR Methods).

The transcription factors *Spi1* and *Irf8* have been shown to be the core orchestrators for microglia development (Hoeffel et al., 2015; Kierdorf et al., 2013). *Tgfbr2* and *Csf1r* have also been demonstrated to play an essential signaling role in microglia development, where the absence of these genes or inhibition of their signaling shows marked reduction or complete absence of microglia (Cohen et al., 2014; Cronk et al., 2018; Elmore et al., 2014; Matcovitch-Natan et al., 2016; Pridans et al., 2018). *CSF1R* mutations also reduce microglia numbers in the human brain (Colonna and Butovsky, 2017). Consistent with these results, we observed strong conservation and expression of *Spi1*, *Irf8*, *Csf1r*, and *Tgfbr2* across all species, supporting the idea of a central role of these factors in microglia biology (Figures 3A, 3B, and S3C). Lysosomal hydrolases (e.g., *Cst3*, *Ctsa*, *Ctss*, *Ctsb*, *Ctsh*, *Ctsc*, *Ctsz*, and *Hexa*) were observed to be both highly expressed and conserved across mammalian species. Several of them are ubiquitously expressed in macrophages (e.g., *Ctsb*, *Ctsh*, and *Ctsc*), but others have more restricted tissue expression, and their absence (e.g., *Ctsa* and *Hexa*) can cause severe neurological phenotypes (Caciotti et al., 2013). Another highly expressed and conserved lysosomal gene, *Grn* (or progranulin), has been implicated in frontotemporal dementia in humans and mice (Baker et al., 2006).

Microglia genes that have been linked previously to the homeostatic gene signature of microglia are both highly expressed and conserved in all species, including *C1qc*, *P2ry12*, and *Tardbp* (Figures 3B, 3C, and S3C). *Tardbp* has been shown recently to be protective against synapse loss in an AD mouse model, whereas its absence promotes higher amyloid clearance by enhancing phagocytosis (Paolicelli et al., 2017). *Vsir* (or VISTA) is an immune checkpoint gene that inhibits T cell response (Xu et al., 2018) and is highly conserved in all microglia (Figures 3C and S3C). Its expression has been shown to be increased in several neurological diseases, such as AD (Borggrewe et al., 2018). Interestingly, previously identified markers for yolk-sac-derived microglia (e.g., *Daglb*, *Bin1*, *Cst3*, *Sall1*, *Prpsap2*, *Entpd1*, *Tmem119*, *P2ry12*, and *CD81*; Figures 3B, 3C, and S3C) were present in core microglia clusters 1–3. These genes are highly enriched in microglia and are not upregulated in monocytes that engraft the brain in microglia-depleted mouse models (Bennett et al., 2018; Cronk et al., 2018; Shemer et al., 2018).

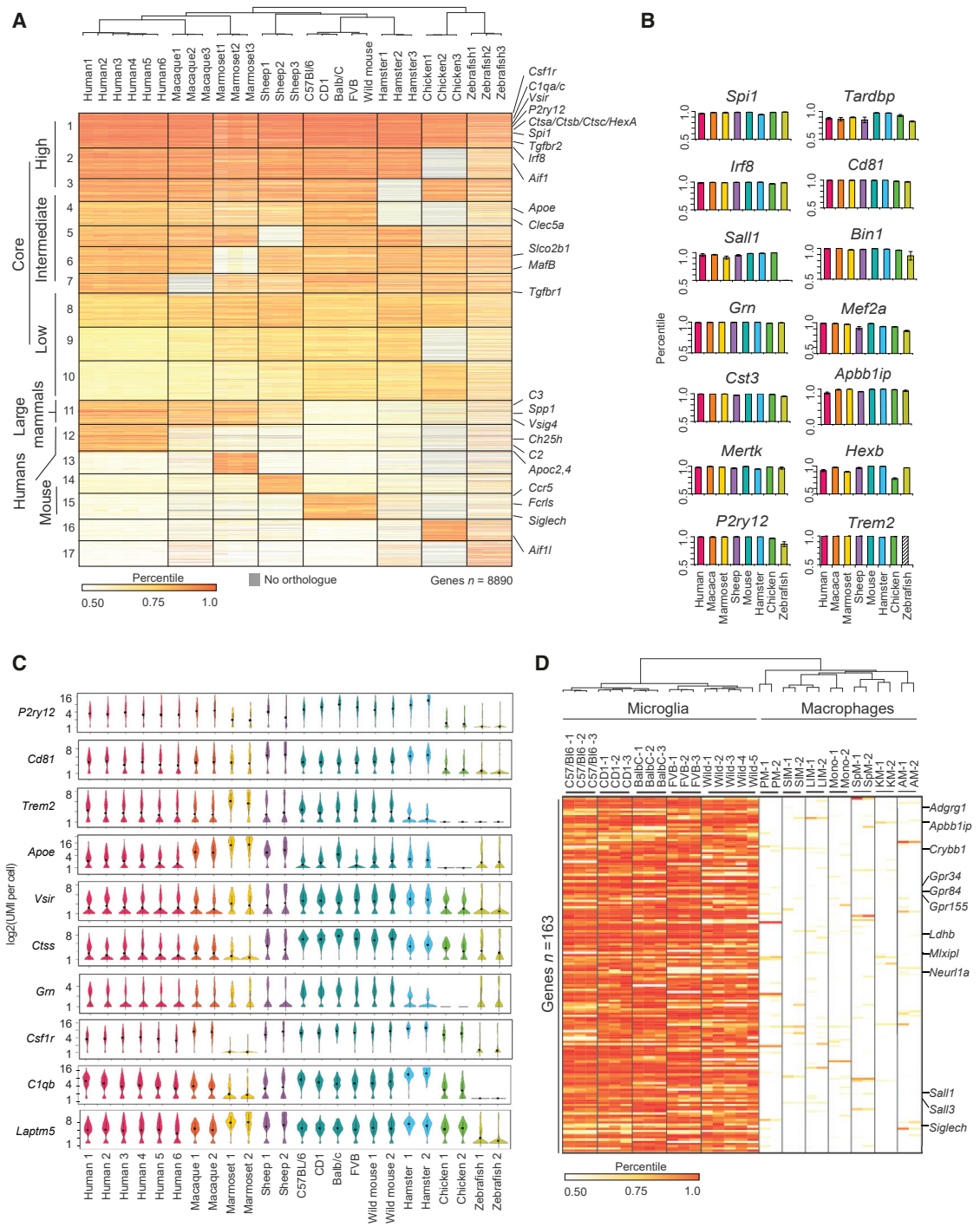

Figure 3. Conserved Microglia Core Gene Expression Program across Evolution

(A) Heatmap representation of ranked bulk RNA-seq expression of *in silico*-deconvoluted microglia. Genes are clustered by the most differential gene expression (k-means = 17), with a representative dendrogram showing nested groups of microglia genes measured by Pearson's correlation coefficient. Shown are annotations of shared and differential profile signatures over species, considering the top 50% (0.50 percentile) of all genes in the gene-set as a fixed expression threshold (by row). Non-expressed and lowly expressed genes are in the lowest percentile (0.5–0.67), medium expressed genes in the mean percentile (0.68–0.85), and highest expressed genes in the top percentile (0.86–1.0). Biological replicates; human microglia (n = 6), marmoset microglia (n = 3), macaque microglia (n = 3), hamster microglia (n = 3), sheep microglia (n = 3), chicken (n = 3), zebrafish (n = 3, five pooled brains each), mouse microglia (one individual from each strain is depicted; n = 3 for C57BL/6, CD1, BALB/c, and FVB, n = 5 for wild mice).

(legend continued on next page)

Many of the conserved microglia genes in clusters 1–3 are shared by other tissue macrophages, which underlines the sentient role of microglia/macrophages as phagocytic and defense cells in multicellular organisms (Figure S3F; Table S4). In order to identify the conserved microglia-specific genes, we next compared our cross-species core signature (clusters 1–3) to previously published datasets of a large compendium of mouse tissue macrophages (Lavin et al., 2014). This was done with the aim to discover highly conserved and cross-species genes specific for microglia but not other tissue macrophages (Lavin et al., 2014). Our cross-species analysis identified 163 genes that are both conserved and unique to microglia (Figure 3D; Table S4; Lavin et al., 2014). Among them is *Adgrg1* (*Gpr56*), demonstrated previously to be conserved in human, mouse, and zebrafish, which is associated with development of oligodendrocytes (Giera et al., 2018). Another conserved microglial gene is amyloid β precursor protein-binding family b member 1 interacting protein (*Apbb1ip*) (Figure 3D), a binding partner of amyloid precursor protein (APP), Tau, 14-3-3γ, and glycogen synthase kinase 3 β (GSK3 β). We further identified brain-specific functions; for example, regulation of neuron projection development and cerebellum development, as the most enriched gene ontology pathways associated with these microglia-specific genes (Figure S3G). These results indicate that microglia express a large set of conserved core genes across all mammalian species, including genes relevant for general tissue macrophage functions as well as microglia-specific CNS adaptations. In addition, we could confirm two of those markers, P2RY12 and PU.1, by histology in several animals (Figures S4A and S4B, respectively).

Single-Cell Transcriptomic Analysis Identifies Human Microglia Subsets

In order to examine whether the microglia of each species display a homogeneous cell type or contain several subtypes, we further analyzed the microglia single-cell data to evaluate microglia heterogeneity for each mammalian species. We first clustered microglia cells from each species separately and compared the intra- versus inter-cluster correlation to evaluate whether there is a clear separation of microglia sub-types or a continuum of a single population (Figure 4A). Surprisingly, we observed low inter-cluster correlation in all human samples compared with intra-clusters (Figure 4A). Cell-to-cell correlation analysis revealed that microglia from all human individuals are organized into several microglia types (Figure 4B), which confirms previous reports (Masuda et al., 2019). These subtypes are unrelated to sex differences and observed in both male and female microglia (Table S1; Figure 4B). The human microglia heterogeneity identified was in sharp contrast to mouse (Figure 4C), macaque (Figure S5A), marmoset (Figure S5B), hamster (Figure S5C), and sheep (Figure S5D), which show high intra-cluster correlation and predominantly one dominant microglia type. Probing the heterogeneity of human microglia, we observed a sub-population with increased expression of several inflammatory genes that have been linked with a senescence-associated secretory phenotype (SASP) (von Kobbe, 2018; Figure 4D), without any change of homeostatic gene expression (Figure 4D). This inflammatory signature of potentially senescent-like microglia has been identified in most tissues of all ages in human and mice, but their number increases with age (He and Sharpless, 2017). These cells are implicated in sterile inflammation, wound healing, and age-related processes, including neurodegeneration (Bussian et al., 2018). Further investigation of these putative senescent-like microglia revealed that they were not specific to a single individual but consistent across all six sampled individuals, comprising roughly 20% of all microglia (Figures 4B and 4E). This microglia subset consistently co-expressed *CDKN1*, *CCL3*, *CCL4*, *CCL3L3*, and *CCL4L2* (Figure 4F), along with higher expression of inflammatory cytokines such as *TNF* and *IL1B* (Figures 4B and 4D). This signature was not observed in young adult mouse microglia (Figure 4C), but inflammatory cytokines have been seen previously in a sub-set of microglia in aged C57BL/6 mice (Hammond et al., 2019; Sierra et al., 2007; Mrdjen et al., 2018).

A potential source of human microglia heterogeneity may involve interaction with the non-sterile environment. However, we did not observe microglia heterogeneity in wild mice (Figure S5E). Laboratory mouse models have been described to show considerable differences regarding the immune system regulation (Sellers et al., 2012). Nevertheless, the microglia expression program of all mouse strains showed high similarity to each other (Figure S5F), and only a few genes were identified as differential between the mouse strains (Figure S5G) Furthermore, comparing non-challenged microglia from four laboratory mouse strains housed in a specific pathogen-free (SPF) facility, with wild mice housed in a non-SPF facility (including pathogens that are present in a natural environment), revealed only few differences (Figure S5H). In summary, single-cell transcriptomic analysis identifies major microglia heterogeneity in humans, in contrast to other mammals, which mostly display a single microglia type in the steady state under non-pathological conditions.

Inter-species Comparison Identifies Divergence in Metabolic and Immune Pathways

In order to better understand the conservation of genes associated with neurodegenerative diseases, we have expanded our single-cell analysis to include two additional rodent models, the rat (*Rattus norvegicus*) and the long-lived blind mole rat (BMR, *Spalax ehrenbergi*; reported life span of over 20 years) (Figures 5A, S6A, and S6B). Pairwise comparison of human microglia scRNA-seq transcriptomics data with those of rodents identified a large number of differentially expressed genes (Figures 5A and

(B) Bar plots of ranked bulk RNA-seq expression of highly conserved and highly expressed genes identified in cluster 1 (as shown in A). Genes with no orthologs are marked with a diagonally striped bar. Error bars show SD.

(C) Violin-plots showing the median (black dot) and distribution of scRNA-seq gene expression (unique molecular identifier [UMI] count) across different replicates and species.

(D) Heatmap of mean gene expression of mouse microglia genes in clusters 1–3 (left panel, highly conserved genes) compared with gene sets of mouse tissue macrophages as described in Lavin et al. (2014) (right panel). The most differentially expressed genes are depicted (163 genes of a total of 1,791 genes from clusters 1–3).

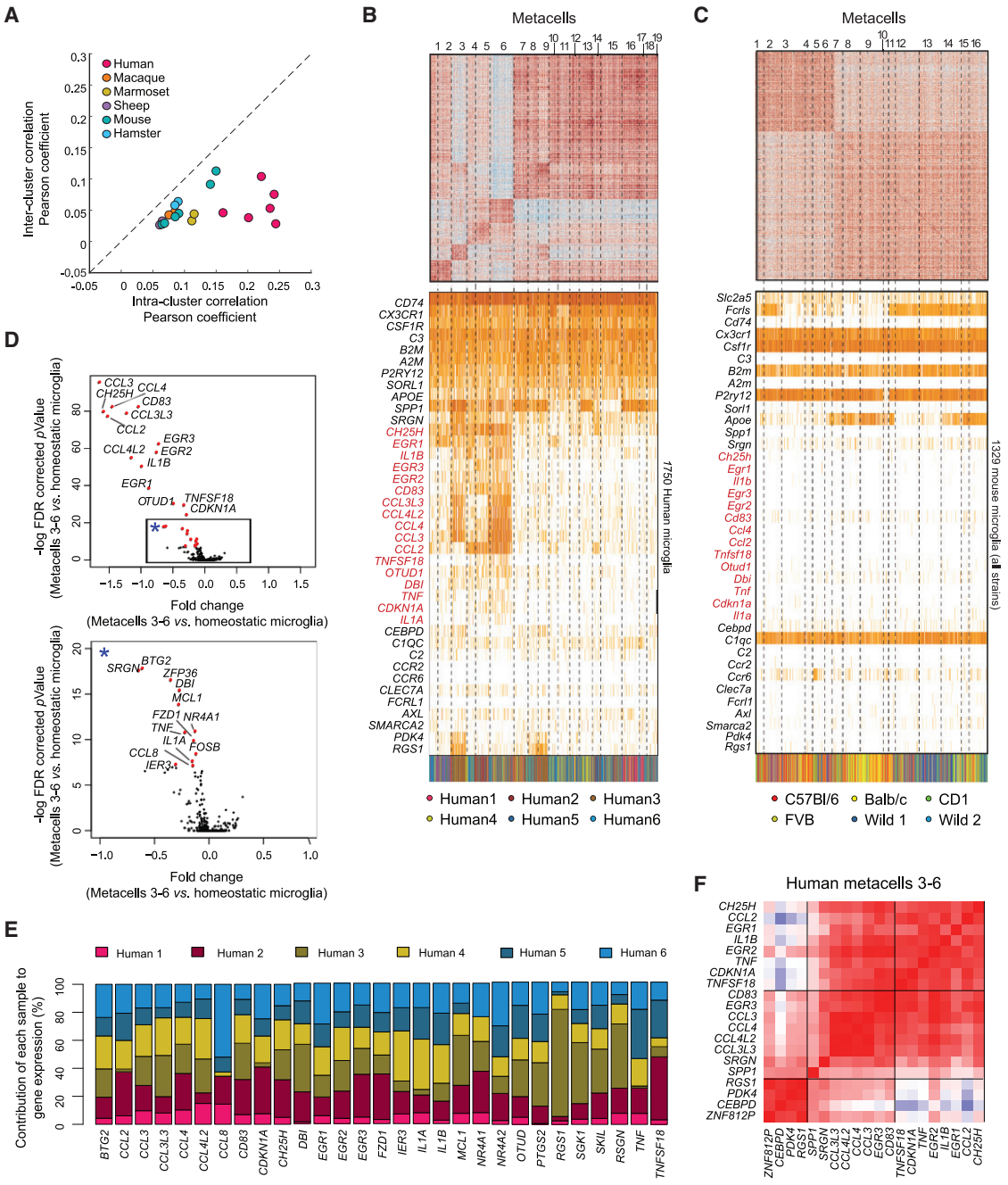

Figure 4. Identification of Microglia Heterogeneity Using Single-Cell RNA-Seq Analysis

(A) Scatterplot showing the relationship between inter- and intra-cluster correlation (Pearson correlation, r_s) of species.

(B and C) Cell-to-cell correlation plot of microglia and corresponding heatmap for the most differentially expressed genes. In the heatmap, each mark represents one metacell, and each row marks a metacell from one individual.

(B) Human microglia (n = 6). Color barcoding marks each human individual at the bottom of the respective row.

(C) Microglia from wild mice (n = 5). Color barcoding marks each mouse strain analyzed. Dotted vertical lines represent separation into metacells.

(D) Top panel: volcano plot showing the most differential genes between homeostatic microglia and microglia subtypes (metacells 3–6, $p < 10^{-7}$). Bottom panel: magnification of specific genes for clarity.

(E) Stack bar graph showing the contribution (percent) of each human sample to the corresponding expression of the putative senescent-like genes.

(F) Gene-gene correlation heatmap of the senescent-like cluster in human microglia (metacells 3–6). Red shows high correlation; blue shows anti-correlation.

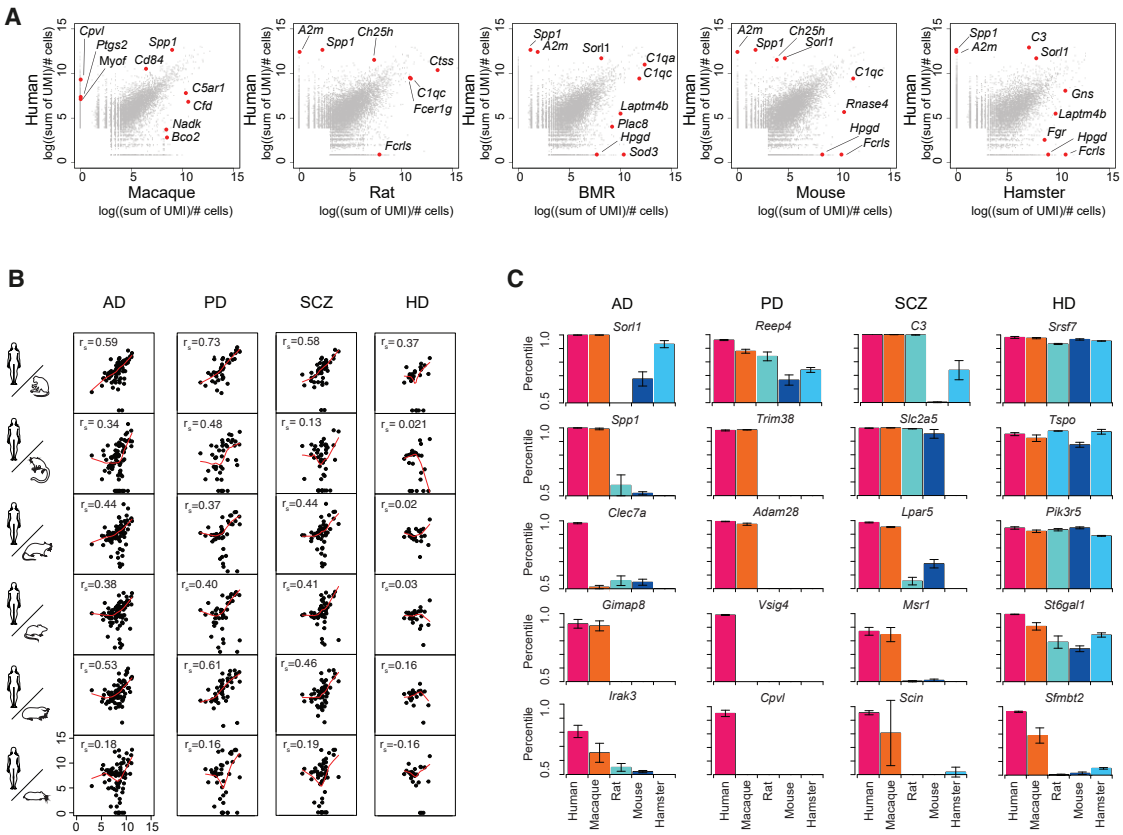

Figure 5. Inter-species Comparison of Homeostatic Microglia Uncovers Species Differences

(A) Scatterplot showing inter-species microglia gene expression. Gene expression is calculated as log (sum of UMI)/number of cells. The genes related to the non-homeostatic subtypes of human microglia (from Figure 4) were removed from the analysis. A subset of differentially expressed genes and marker genes is highlighted in red.

(B) Spearman correlation of scRNA-seq expression (UMI count) of susceptibility genes for (from left to right) AD susceptibility genes, PD susceptibility genes, schizophrenia (SCZ), and Huntington's disease (HD). Species from top to bottom: human versus macaque, human versus marmoset, human versus rat, human versus mouse, human versus BMR, and human versus hamster.

(C) Bar plots showing average and ranked scRNA-seq gene expression (percentile) across human, macaque, rat, mouse, and hamster in AD, PD, SCZ, and HD. Error bars show SD.

S6C; Table S5). In contrast, we observed a considerably smaller number of differentially expressed genes between human and macaque microglia, with most of the differentially expressed genes related to metabolic pathways such as NAD kinase (*NADK*; soluble vitamin metabolism) and beta-carotene oxygenase 2 (*BCO2*; carotenoid oxidization) (Figure 5A).

Pathway analysis of clusters specific to humans, macaque, marmoset, and sheep compared with rodents revealed enrichment of DNA repair pathways (Figure S6D), which have been implicated previously in longevity (Ungvari et al., 2008). Additionally, enriched pathways included phagocytosis (Figure S6E)—more specifically, apoptotic cell clearance (Figure S6F; Table S6)—and the complement pathway (STAR Methods; Figure S6G; Table S6). Several other pathways were enriched in all tested mammals except mice; in particular, negative regulation of the ferroptosis pathway (Figure S6H). Ferroptosis is a newly described form of cell death driven by loss of activity of the lipid repair enzyme glutathione peroxidase 4 (*GPX4*) and subsequent accumulation of lipid-based reactive oxygen species (ROS), along with cytosolic accumulation of iron. Interestingly, several of those cellular events, including defects in phagocytosis, are thought to be hallmark drivers of many neurodegenerative diseases, including AD and PD.

Conservation and Divergence of Microglia Neurodegeneration-Related Pathways

Rodent animal models are critical for our understanding of many physiological and disease mechanisms. However, successful translation from neurodegenerative animal models to human clinical trials is far from adequate (Doody, 2017; Sperling et al., 2014; Vellas et al., 2014). In order to better understand the conservation of microglia genes associated with neurodegenerative diseases, we compared human microglia with commonly used animal models. We compared the gene expression of neurodegenerative disease susceptibility genes from GWASs of human microglia with those of other mammalian species (STAR Methods; Figure 5B). Expression of PD and AD-associated

genes in human microglia showed the highest correlation with macaque (PD, r = 0.73; AD, r = 0.59) (Figure 5B). In contrast, mice, rats, and hamsters showed moderate to low correlation with human AD and PD susceptibility genes (r = 0.16–0.40) (Figure 5B). We observed significant over-representation of PD genes and, to a lesser extent, AD genes in the human-specific cluster and clusters shared by human and macaques (Figures S6I and S6J). Conversely, we did not see any significant enrichment or depletion of genes from GWASs of schizophrenia or Huntington's disease in any animal (Figures 5B, S6K, and S6L). Human- and macaque-specific susceptibility genes included *Msr1* (macrophage scavenger receptor 1; Figures 5C and S6O). *Msr1* mediates endocytosis of low-density lipoproteins (LDLs) and is involved in uptake and degradation of amyloid β (Aβ) (Frenkel et al., 2013). Previously, genes expressed by microglia have been implicated in AD in human GWASs (Gandal et al., 2018; Jansen et al., 2019; Keren-Shaul et al., 2017). However, this is the first study identifying specific enrichment of AD and PD susceptibility genes in microglia and their expression across evolution (Figures S6I, S6J, S6M, and S6N). In summary, our analysis identifies marked evolution in the expression of multiple microglia pathways involved in metabolic, complement, and phagocytic pathways, with many of these pathways implicated in neurodegenerative diseases.

DISCUSSION

Effective development of therapies for neurodegenerative diseases is limited. This could be due to the complexity of the CNS or, potentially, from lack of molecular understanding of relevant animal models. In the current study, we systematically and comprehensively characterized microglia from ten species of varying evolutionary distance, using a combination of single-cell genomic technologies and histological analysis. We observed conservation of mammalian microglia gene expression programs, suggesting that microglia perform overall similar functions throughout mammalian evolution. This is in accordance with previous reports showing high constraints of brain gene expression variance across evolution (Chan et al., 2009; Brawand et al., 2011; Chen et al., 2019). Nevertheless, a substantial number of species-specific gene expression was observed that exhibited enrichment of several pathways that have not been related previously to microglia or human microglia. Our analysis of human, macaque, and marmoset revealed higher expression of pathways that have been implicated in longevity and anti-inflammatory responses; more specifically, DNA repair pathways, negative regulation of ferroptosis, and apoptotic cell clearance. Many hallmarks of human neurodegeneration specifically involve an increased presence of double-strand DNA damage and senescent cells as well as accumulation of iron and peroxidation of polyunsaturated fatty acids in CNS cells (Fielder et al., 2017; Maynard et al., 2015; Sfera et al., 2018). These putative longevity pathways could shed some light on the molecular basis of homeostatic microglial brain maintenance in long-living animals such as humans. Our analysis additionally revealed that human microglia express the great majority of genes related to susceptibility to AD and PD (but not to Huntington's disease or schizophrenia), whereas rodent microglia only express a fraction of these genes.

We identify substantial heterogeneity in human microglia as well as a sub-cluster of human microglia that expressed a complex SASP that is thought to play a role in homing of immune cells for clearance of senescent cells (Lopes-Paciencia et al., 2019). Regulation of SASP has been linked to several pathways, such as DNA damage response and activation of immune response (Ito et al., 2017). As with any studies involving human tissue, especially the CNS, caution has to be exercised when interpreting the results. Although we took great care and carefully calibrated sample acquisition and processing time (STAR Methods), it cannot be excluded that patients' microglia are not accurately recapitulating the *in situ* states of healthy brains. Nonetheless, comparable studies of human and mouse microglia with a more extensive disease range (epilepsy, brain tumors, or acute ischemia) showed very similar results (Gosselin et al., 2017; Masuda et al., 2019). This supports our argument for human microglia heterogeneity that is not observed to this extent in other species. In summary, our analysis identifies the microglia gene program across evolution. It also provides a fundamental resource to compare microglia over a large evolutionary scale and to guide future development and improvements in understanding of our laboratory models of diseases mediated by microglia dysfunction.

STAR★METHODS

Detailed methods are provided in the online version of this paper and include the following:

- KEY RESOURCES TABLE
- LEAD CONTACT AND MATERIALS AVAILABILITY
- EXPERIMENTAL MODEL AND SUBJECT DETAILS
  - Experimental animals
  - Human samples
- METHOD DETAILS
  - Sample processing
  - Sample processing for histology and FACS
  - Histology
  - Flowcytometry single cell sorting
  - Flowcytometry bulk cell sorting
  - Flowcytometry antibody table
  - Massively Parallel Single-Cell RNA-seq Library preparation (MARS-seq2.0)
  - Bulk RNA-seq library preparation
- QUANTIFICATION AND STATISTICAL ANALYSIS
  - Three-dimensional reconstruction of microglia
  - Bulk low-level processing and filtering
  - Ortholog gene selection
  - Deconvolution of bulk data by detecting single cell outliers
  - Bulk RNA-seq normalization
  - Bulk RNA-seq clustering
  - Gene enrichment analysis
  - Single cells RNA-seq low-level processing and filtering
  - Single cells data processing and clustering
  - Single cell RNA-seq differential expression analysis
  - Pooling single cell RNA-seq data

SUPPLEMENTAL INFORMATION

Supplemental Information can be found online at https://doi.org/10.1016/j.cell.2019.11.010.

ACKNOWLEDGMENTS

We thank Prof. Amos Tanay for important input regarding data analysis and Prof. Claudia Kemper for valuable discussion. We thank Prof. Gil Levkowitz for sharing zebrafish, and Qiyu Chen and Dr. Ludmilla Gordon for valuable technical assistance. We thank Genia Brodsky for artwork and Dr. Bjort Katrinardottir-Kragesteen, Gur Lubin, and Dr. Aleksandra Deszkowska for critical reading of the manuscript. I.A. is an Eden and Steven Romick Professorial Chair, supported by the Chan Zuckerberg Initiative (CZI), an HHMI international scholar award, a European Research Council consolidator grant (ERC-COG 724471-HemTree2.0), an MRA established investigator award (509044), DFG (SFB/TRR167), the Ernest and Bonnie Beutler Research Program for Excellence in Genomic Medicine, Helen and Martin Kimmel awards for innovative investigation, an SCA award of the Wolfson Foundation and Family Charitable Trust, the Thompson Family Foundation Alzheimer's Research Fund, the Adelis Foundation, the Eden and Steven Romick Post-Doctoral Fellowship Fund, and the International Progressive MS Alliance (PA-1604-08459). D.E. is supported by the DFG (SFB/TRR167) and the Berta Ottenstein Programme for Clinician Scientists. M.P. is supported by the Sobek Foundation, the Ernst-Jung Foundation, the DFG (SFB 992, SFB1160, SFB/TRR167, and a Reinhart Koselleck grant), and the Ministry of Science, Research and Arts, Baden-Wuerttemberg (Sonderlinie "Neuroinflammation"). This study was supported by the DFG under Germany's Excellence Strategy (CIBSS, EXC-2189, Project ID 390939984). T.K. is supported by the ISF (grant 1324/15) and the Minerva Foundation and supervised the BMR part of the study. A.B. was supported by the Biotechnology and Biological Sciences Research Council of the United Kingdom through grants from the Institute Strategic Programme (BBS/E/D/10002071). F.G is an EMBO YIP awardee and is supported by Singapore Immunology Network (SIgN) core funding as well as a Singapore National Research Foundation senior investigatorship (NRFI; NRF2016NRF-NRFI001-02). Raw and processed single-cell and bulk RNA sequencing data will be downloaded from NCBI (GEO: GSE134707).

AUTHOR CONTRIBUTIONS

Conceptualization, L.G., D.E., H.K.-S., M.P., and I.A.; Methodology, L.G., D.E., H.K.-S., A.W., and E.D.; Investigation, L.G., D.E., and H.K.-S.; Validation, L.G., D.E., H.K.-S., A.W., S.C.B., J.N., F.S., N.Z., and A.R.-R.; Genomic Data Analysis, E.D., A.W., I.U., L.G.; Image Data Analysis, D.E., M.P., and I.A.; Resources, I.A., M.P., F.G., T.K., C. Stadelmann, F.R.T., C. Scheiwe, K.M., J.V., F.P., C.P., C.A.-D., and A.B.; Data Curation, E.D.; Writing – Original Draft; L.G. and I.A.; Writing – Reviewing & Editing, I.A., H.K.-S., A.W., and L.G.; Visualization, L.G., D.E., E.D., and H.K.-S.; Supervision, M.P.; Figures 1, S1, and S4, I.A.; Figures 2, 3, 4, 5, S2, S3, S5, and S6 and Funding Acquisition: M.P. and I.A.

DECLARATION OF INTEREST

The authors declare no competing interests.

Received: March 12, 2019
Revised: July 30, 2019
Accepted: November 6, 2019
Published: December 12, 2019; corrected online: March 13, 2020; corrected online: April 16, 2020

REFERENCES

Ajami, B., Bennett, J.L., Krieger, C., McNagny, K.M., and Rossi, F.M.V. (2011). Infiltrating monocytes trigger EAE progression, but do not contribute to the resident microglia pool. Nat. Neurosci. *14*, 1142–1149.

Alliot, F., Godin, I., and Pessac, B. (1999). Microglia derive from progenitors, originating from the yolk sac, and which proliferate in the brain. Brain Res. Dev. Brain Res. *117*, 145–152.

Askew, K., Li, K., Olmos-Alonso, A., Garcia-Moreno, F., Liang, Y., Richardson, P., Tipton, T., Chapman, M.A., Riecken, K., Beccari, S., et al. (2017). Coupled proliferation and apoptosis maintain the rapid turnover of microglia in the adult brain. Cell Rep. *18*, 391–405.

Baker, M., Mackenzie, I.R., Pickering-Brown, S.M., Gass, J., Rademakers, R., Lindholm, C., Snowden, J., Adamson, J., Sadovnick, A.D., Rollinson, S., et al. (2006). Mutations in progranulin cause tau-negative frontotemporal dementia linked to chromosome 17. Nature *442*, 916–919.

Balic, A., Garcia-Morales, C., Vervelde, L., Gilhooley, H., Sherman, A., Garceau, V., Gutowska, M.W., Burt, D.W., Kaiser, P., Hume, D.A., and Sang, H.M. (2014). Visualisation of chicken macrophages using transgenic reporter genes: insights into the development of the avian macrophage lineage. Development *141*, 3255–3265.

Baran, Y., Sebé-Pedrós, A., Lubling, Y., Giladi, A., Chomsky, E., Meir, Z., Hoichman, M., Lifshitz, A., and Tanay, A. (2018). MetaCell: analysis of single cell RNA-seq data using k-NN graph partitions. Genome Biol. *20*, 206.

Baron, M., Veres, A., Wolock, S.L., Faust, A.L., Gaujoux, R., Vetere, A., Ryu, J.H., Wagner, B.K., Shen-Orr, S.S., Klein, A.M., et al. (2016). A single-cell transcriptomic map of the human and mouse pancreas reveals inter- and intra-cell population structure. Cell Syst. *3*, 346–360.e4.

Bennett, F.C., Bennett, M.L., Yaqoob, F., Mulinyawe, S.B., Grant, G.A., Hayden Gephart, M., Plowey, E.D., and Barres, B.A. (2018). A combination of ontogeny and CNS environment establishes microglial identity. Neuron *98*, 1170–1183.e8.

Borggrewe, M., Grit, C., Den Dunnen, W.F.A., Burm, S.M., Bajramovic, J.J., Noelle, R.J., Eggen, B.J.L., and Laman, J.D. (2018). VISTA expression by microglia decreases during inflammation and is differentially regulated in CNS diseases. Glia *66*, 2645–2658.

Brawand, D., Soumillon, M., Necsulea, A., Julien, P., Csárdi, G., Harrigan, P., Weier, M., Liechti, A., Aximu-Petri, A., Kircher, M., et al. (2011). The evolution of gene expression levels in mammalian organs. Nature *478*, 343–348.

Bruttger, J., Karram, K., Wörtge, S., Regen, T., Marini, F., Hoppmann, N., Klein, M., Blank, T., Yona, S., Wolf, Y., et al. (2015). Genetic cell ablation reveals clusters of local self-renewing microglia in the mammalian central nervous system. Immunity *43*, 92–106.

Bussian, T.J., Aziz, A., Meyer, C.F., Swenson, B.L., van Deursen, J.M., and Baker, D.J. (2018). Clearance of senescent glial cells prevents tau-dependent pathology and cognitive decline. Nature *562*, 578–582.

Caciotti, A., Catarzi, S., Tonin, R., Lugli, L., Perez, C.R., Michelakakis, H., Mavridou, I., Donati, M.A., Guerrini, R., d'Azzo, A., and Morrone, A. (2013). Galactosialidosis: review and analysis of CTSA gene mutations. Orphanet J. Rare Dis. *8*, 114.

Chan, E.T., Quon, G.T., Chua, G., Babak, T., Trochesset, M., Zirngibl, R.A., Aubin, J., Ratcliffe, M.J.H., Wilde, A., Brudno, M., et al. (2009). Conservation of core gene expression in vertebrate tissues. J. Biol. *8*, 33.

Chen, J., Swofford, R., Johnson, J., Cummings, B.B., Rogel, N., Lindblad-Toh, K., Haerty, W., Palma, F.D., and Regev, A. (2019). A quantitative framework for characterizing the evolutionary history of mammalian gene expression. Genome Res. *29*, 53–63.

Cohen, M., Matcovitch, O., David, E., Barnett-Itzhaki, Z., Keren-Shaul, H., Blecher-Gonen, R., Jaitin, D.A., Sica, A., Amit, I., and Schwartz, M. (2014). Chronic exposure to TGFβ1 regulates myeloid cell inflammatory response in an IRF7-dependent manner. EMBO J. *33*, 2906–2921.

Colonna, M., and Butovsky, O. (2017). Microglia function in the central nervous system during health and neurodegeneration. Annu. Rev. Immunol. *35*, 441–468.

Cronk, J.C., Filiano, A.J., Louveau, A., Marin, I., Marsh, R., Ji, E., Goldman, D.H., Smirnov, I., Geraci, N., Acton, S., et al. (2018). Peripherally derived macrophages can engraft the brain independent of irradiation and maintain an identity distinct from microglia. J. Exp. Med. *215*, 1627–1647.

Doody, R. (2017). Developing disease-modifying treatments in Alzheimer's disease - a perspective from Roche and Genentech. J. Prev. Alzheimers Dis. *4*, 264–272.

Drago, F., Sautière, P.-E., Le Marrec-Croq, F., Accorsi, A., Van Camp, C., Salzet, M., Lefebvre, C., and Vizioli, J. (2014). Microglia of medicinal leech (Hirudo medicinalis) express a specific activation marker homologous to vertebrate ionized calcium-binding adapter molecule 1 (Iba1/alias aif-1). Dev. Neurobiol. *74*, 987–1001.

Drew, L. (2018). An age-old story of dementia. Nature *559*, S2–S3.

Ellett, F., Pase, L., Hayman, J.W., Andrianopoulos, A., and Lieschke, G.J. (2011). mpeg1 promoter transgenes direct macrophage-lineage expression in zebrafish. Blood *117*, e49–e56.

Elmore, M.R.P., Najafi, A.R., Koike, M.A., Dagher, N.N., Spangenberg, E.E., Rice, R.A., Kitazawa, M., Matusow, B., Nguyen, H., West, B.L., and Green, K.N. (2014). Colony-stimulating factor 1 receptor signaling is necessary for microglia viability, unmasking a microglia progenitor cell in the adult brain. Neuron *82*, 380–397.

Erny, D., Hrabě de Angelis, A.L., Jaitin, D., Wieghofer, P., Staszewski, O., David, E., Keren-Shaul, H., Mahlakoiv, T., Jakobshagen, K., Buch, T., et al. (2015). Host microbiota constantly control maturation and function of microglia in the CNS. Nat. Neurosci. *18*, 965–977.

Fielder, E., von Zglinicki, T., and Jurk, D. (2017). The DNA damage response in neurons: die by apoptosis or survive in a senescence-like state? J. Alzheimers Dis. *60* (s1), S107–S131.

Frenkel, D., Wilkinson, K., Zhao, L., Hickman, S.E., Means, T.K., Puckett, L., Farfara, D., Kingery, N.D., Weiner, H.L., and El Khoury, J. (2013). Scara1 deficiency impairs clearance of soluble amyloid-β by mononuclear phagocytes and accelerates Alzheimer's-like disease progression. Nat. Commun. *4*, 2030.

Gandal, M.J., Haney, J.R., Parikshak, N.N., Leppa, V., Ramaswami, G., Hartl, C., Schork, A.J., Appadurai, V., Buil, A., Werge, T.M., et al.; CommonMind Consortium; PsychENCODE Consortium; iPSYCH-BROAD Working Group (2018). Shared molecular neuropathology across major psychiatric disorders parallels polygenic overlap. Science *359*, 693–697.

Giera, S., Luo, R., Ying, Y., Ackerman, S.D., Jeong, S.-J., Stoveken, H.M., Folts, C.J., Welsh, C.A., Tall, G.G., Stevens, B., et al. (2018). Microglial transglutaminase-2 drives myelination and myelin repair via GPR56/ADGRG1 in oligodendrocyte precursor cells. eLife *7*, 6122.

Giladi, A., and Amit, I. (2018). Single-cell genomics: a stepping stone for future immunology discoveries. Cell *172*, 14–21.

Giladi, A., Paul, F., Herzog, Y., Lubling, Y., Weiner, A., Yofe, I., Jaitin, D., Cabezas-Wallscheid, N., Dress, R., Ginhoux, F., et al. (2018). Single-cell characterization of haematopoietic progenitors and their trajectories in homeostasis and perturbed haematopoiesis. Nat. Cell Biol. *20*, 836–846.

Ginhoux, F., Greter, M., Leboeuf, M., Nandi, S., See, P., Gokhan, S., Mehler, M.F., Conway, S.J., Ng, L.G., Stanley, E.R., et al. (2010). Fate mapping analysis reveals that adult microglia derive from primitive macrophages. Science *330*, 841–845.

Gomez Perdiguero, E.G., Klapproth, K., Schulz, C., Busch, K., Azzoni, E., Crozet, L., Garner, H., Trouillet, C., de Bruijn, M.F., Geissmann, F., and Rodewald, H.R. (2015). Tissue-resident macrophages originate from yolk-sac-derived erythro-myeloid progenitors. Nature *518*, 547–551.

Gosselin, D., Link, V.M., Romanoski, C.E., Fonseca, G.J., Eichenfield, D.Z., Spann, N.J., Stender, J.D., Chun, H.B., Garner, H., Geissmann, F., and Glass, C.K. (2014). Environment drives selection and function of enhancers controlling tissue-specific macrophage identities. Cell *159*, 1327–1340.

Gosselin, D., Skola, D., Coufal, N.G., Holtman, I.R., Schlachetzki, J.C.M., Sajti, E., Jaeger, B.N., O'Connor, C., Fitzpatrick, C., Pasillas, M.P., et al. (2017). An environment-dependent transcriptional network specifies human microglia identity. Science *356*, 1248–1259.

Hammond, T.R., Dufort, C., Dissing-Olesen, L., Giera, S., Young, A., Wysoker, A., Walker, A.J., Gergits, F., Segel, M., Nemesh, J., et al. (2019). Single-Cell RNA Sequencing of Microglia throughout the Mouse Lifespan and in the Injured Brain Reveals Complex Cell-State Changes. Immunity *50*, 253–271.

Hashimoto, D., Chow, A., Noizat, C., Teo, P., Beasley, M.B., Leboeuf, M., Becker, C.D., See, P., Price, J., Lucas, D., et al. (2013). Tissue-resident macrophages self-maintain locally throughout adult life with minimal contribution from circulating monocytes. Immunity *38*, 792–804.

He, S., and Sharpless, N.E. (2017). Senescence in Health and Disease. Cell *169*, 1000–1011.

Hoeffel, G., Chen, J., Lavin, Y., Low, D., Almeida, F.F., See, P., Beaudin, A.E., Lum, J., Low, I., Forsberg, E.C., et al. (2015). C-Myb(+) erythro-myeloid progenitor-derived fetal monocytes give rise to adult tissue-resident macrophages. Immunity *42*, 665–678.

Holmes, N. (2006). CD45: all is not yet crystal clear. Immunology *117*, 145–155.

Ito, Y., Hoare, M., and Narita, M. (2017). Spatial and temporal control of senescence. Trends Cell Biol. *27*, 820–832.

Jaitin, D.A., Kenigsberg, E., Keren-Shaul, H., Elefant, N., Paul, F., Zaretsky, I., Mildner, A., Cohen, N., Jung, S., Tanay, A., and Amit, I. (2014). Massively parallel single-cell RNA-seq for marker-free decomposition of tissues into cell types. Science *343*, 776–779.

Jaitin, D.A., Adlung, L., Thaiss, C.A., Weiner, A., Li, B., Descamps, H., Lundgren, P., Bleriot, C., Liu, Z., Deczkowska, A., et al. (2019). Lipid-associated macrophages control metabolic homeostasis in a Trem2-dependent manner. Cell *178*, 686–698.e14.

Jansen, I.E., Savage, J.E., Watanabe, K., Bryois, J., Williams, D.M., Steinberg, S., Sealock, J., Karlsson, I.K., Hägg, S., Athanasiu, L., et al. (2019). Genome-wide meta-analysis identifies new loci and functional pathways influencing Alzheimer's disease risk. Nat. Genet. *51*, 404–413.

Keren-Shaul, H., Spinrad, A., Weiner, A., Matcovitch-Natan, O., Dvir-Szternfeld, R., Ulland, T.K., David, E., Baruch, K., Lara-Astaiso, D., Toth, B., et al. (2017). A unique microglia type associated with restricting development of Alzheimer's disease. Cell *169*, 1276–1290.e17.

Keren-Shaul, H., Kenigsberg, E., Jaitin, D.A., David, E., Paul, F., Tanay, A., and Amit, I. (2019). MARS-seq2.0: an experimental and analytical pipeline for indexed sorting combined with single-cell RNA sequencing. Nature Protocols *14*, 1841–1862.

Kierdorf, K., Erny, D., Goldmann, T., Sander, V., Schulz, C., Perdiguero, E.G., Wieghofer, P., Heinrich, A., Riemke, P., Hölscher, C., et al. (2013). Microglia emerge from erythromyeloid precursors via Pu.1- and Irf8-dependent pathways. Nat. Neurosci. *16*, 273–280.

Kim, D., Langmead, B., and Salzberg, S.L. (2015). HISAT: a fast spliced aligner with low memory requirements. Nat. Methods *12*, 357–360.

Kryuchkova-Mostacci, N., and Robinson-Rechavi, M. (2016). Tissue-specificity of gene expression diverges slowly between orthologs, and rapidly between paralogs. PLoS Comput. Biol. *12*, e1005274.

La Manno, G., Gyllborg, D., Codeluppi, S., Nishimura, K., Salto, C., Zeisel, A., Borm, L.E., Stott, S.R.W., Toledo, E.M., Villaescusa, J.C., et al. (2016). Molecular diversity of midbrain development in mouse, human, and stem cells. Cell *167*, 566–580.e19.

Lambert, J.C., Ibrahim-Verbaas, C.A., Harold, D., Naj, A.C., Sims, R., Bellenguez, C., DeStafano, A.L., Bis, J.C., Beecham, G.W., Grenier-Boley, B., et al.; European Alzheimer's Disease Initiative (EADI); Genetic and Environmental Risk in Alzheimer's Disease; Alzheimer's Disease Genetic Consortium; Cohorts for Heart and Aging Research in Genomic Epidemiology (2013). Meta-analysis of 74,046 individuals identifies 11 new susceptibility loci for Alzheimer's disease. Nat. Genet. *45*, 1452–1458.

Lavin, Y., Winter, D., Blecher-Gonen, R., David, E., Keren-Shaul, H., Merad, M., Jung, S., and Amit, I. (2014). Tissue-resident macrophage enhancer landscapes are shaped by the local microenvironment. Cell *159*, 1312–1326.

Lawson, L.J., Perry, V.H., Dri, P., and Gordon, S. (1990). Heterogeneity in the distribution and morphology of microglia in the normal adult mouse brain. Neuroscience *39*, 151–170.

Li, H., van der Leun, A.M., Yofe, I., Lubling, Y., Gelbard-Solodkin, D., van Akkooi, A.C.J., van den Braber, M., Rozeman, E.A., Haanen, J.B.A.G., Blank, C.U., et al. (2019). Dysfunctional CD8 T cells form a proliferative, dynamically regulated compartment within human melanoma. Cell *176*, 775–789.e18.

Lopes-Paciencia, S., Saint-Germain, E., Rowell, M.-C., Ruiz, A.F., Kalegari, P., and Ferbeyre, G. (2019). The senescence-associated secretory phenotype and its regulation. Cytokine *117*, 15–22.

Masuda, T., Sankowski, R., Staszewski, O., Böttcher, C., Amann, L., Scheiwe, C., Nessler, S., Kunz, P., van Loo, G., Coenen, V.A., et al. (2019). Spatial and temporal heterogeneity of mouse and human microglia at single-cell resolution. Nature *15*, 300–392.

Matcovitch-Natan, O., Winter, D.R., Giladi, A., Vargas Aguilar, S., Spinrad, A., Sarrazin, S., Ben-Yehuda, H., David, E., Zelada González, F., Perrin, P., et al. (2016). Microglia development follows a stepwise program to regulate brain homeostasis. Science *353*, aad8670.

Maynard, S., Fang, E.F., Scheibye-Knudsen, M., Croteau, D.L., and Bohr, V.A. (2015). DNA damage, DNA repair, aging, and neurodegeneration. Cold Spring Harb. Perspect. Med. *5*, a025130.

Menassa, D.A., and Gomez-Nicola, D. (2018). Microglial dynamics during human brain development. Front. Immunol. *9*, 1014.

Mrdjen, D., Pavlovic, A., Hartmann, F.J., Schreiner, B., Utz, S.G., Leung, B.P., Lelios, I., Heppner, F.L., Kipnis, J., Merkler, D., et al. (2018). High-Dimensional Single-Cell Mapping of Central Nervous System Immune Cells Reveals Distinct Myeloid Subsets in Health, Aging, and Disease. Immunity *48*, 380–395.

Nagata, T., Suzuki, T., Ohta, Y., Flajnik, M.F., and Kasahara, M. (2002). The leukocyte common antigen (CD45) of the Pacific hagfish, Eptatretus stoutii: implications for the primordial function of CD45. Immunogenetics *54*, 286–291.

Najafi, A.R., Crapser, J., Jiang, S., Ng, W., Mortazavi, A., West, B.L., and Green, K.N. (2018). A limited capacity for microglial repopulation in the adult brain. Glia *66*, 2385–2396.

Okumura, M., Matthews, R.J., Robb, B., Litman, G.W., Bork, P., and Thomas, M.L. (1996). Comparison of CD45 extracellular domain sequences from divergent vertebrate species suggests the conservation of three fibronectin type III domains. J. Immunol. *157*, 1569–1575.

Paolicelli, R.C., Jawaid, A., Henstridge, C.M., Valeri, A., Merlini, M., Robinson, J.L., Lee, E.B., Rose, J., Appel, S., Lee, V.M.-Y., et al. (2017). TDP-43 depletion in microglia promotes amyloid clearance but also induces synapse loss. Neuron *95*, 297–308.e6.

Papalexi, E., and Satija, R. (2018). Single-cell RNA sequencing to explore immune cell heterogeneity. Nat. Rev. Immunol. *18*, 35–45.

Parkhurst, C.N., Yang, G., Ninan, I., Savas, J.N., Yates, J.R., 3rd, Lafaille, J.J., Hempstead, B.L., Littman, D.R., and Gan, W.-B. (2013). Microglia promote learning-dependent synapse formation through brain-derived neurotrophic factor. Cell *155*, 1596–1609.

Paul, F., Arkin, Y., Giladi, A., Jaitin, D.A., Kenigsberg, E., Keren-Shaul, H., Winter, D., Lara-Astiaso, D., Gury, M., Weiner, A., et al. (2016). Transcriptional heterogeneity and lineage commitment in myeloid progenitors. Cell *164*, 325.

Perry, V.H. (1998). A revised view of the central nervous system microenvironment and major histocompatibility complex class II antigen presentation. J. Neuroimmunol. *90*, 113–121.

Pollen, A.A., Nowakowski, T.J., Shuga, J., Wang, X., Leyrat, A.A., Lui, J.H., Li, N., Szpankowski, L., Fowler, B., Chen, P., et al. (2014). Low-coverage single-cell mRNA sequencing reveals cellular heterogeneity and activated signaling pathways in developing cerebral cortex. Nat. Biotechnol. *32*, 1053–1058.

Pollen, A.A., Nowakowski, T.J., Chen, J., Retallack, H., Sandoval-Espinosa, C., Nicholas, C.R., Shuga, J., Liu, S.J., Oldham, M.C., Diaz, A., et al. (2015). Molecular identity of human outer radial glia during cortical development. Cell *163*, 55–67.

Pridans, C., Raper, A., Davis, G.M., Alves, J., Sauter, K.A., Lefevre, L., Regan, T., Meek, S., Sutherland, L., Thomson, A.J., et al. (2018). Pleiotropic impacts of macrophage and microglial deficiency on development in rats with targeted mutation of the *Csf1r* locus. J. Immunol. *201*, 2683–2699.

Prinz, M., and Priller, J. (2014). Microglia and brain macrophages in the molecular age: from origin to neuropsychiatric disease. Nat. Rev. Neurosci. *15*, 300–312.

Schafer, D.P., Lehrman, E.K., Kautzman, A.G., Koyama, R., Mardinly, A.R., Yamasaki, R., Ransohoff, R.M., Greenberg, M.E., Barres, B.A., and Stevens, B. (2012). Microglia sculpt postnatal neural circuits in an activity and complement-dependent manner. Neuron *74*, 691–705.

Sebé-Pedrós, A., Saudemont, B., Chomsky, E., Plessier, F., Mailhé, M.-P., Renno, J., Loe-Mie, Y., Lifshitz, A., Mukamel, Z., Schmutz, S., et al. (2018). Cnidarian cell type diversity and regulation revealed by whole-organism single-cell RNA-Seq. Cell *173*, 1520–1534.e20.

Sellers, R.S., Clifford, C.B., Treuting, P.M., and Brayton, C. (2012). Immunological variation between inbred laboratory mouse strains: points to consider in phenotyping genetically immunomodified mice. Vet. Pathol. *49*, 32–43.

Sfera, A., Bullock, K., Price, A., Inderias, L., and Osorio, C. (2018). Ferrosenescence: the iron age of neurodegeneration? Mech. Ageing Dev. *174*, 63–75.

Shemer, A., Grozovski, J., Tay, T.L., Tao, J., Volaski, A., Süß, P., Ardura-Fabregat, A., Gross-Vered, M., Kim, J.-S., David, E., et al. (2018). Engrafted parenchymal brain macrophages differ from microglia in transcriptome, chromatin landscape and response to challenge. Nat. Commun. *9*, 5206.

Sierra, A., de Castro, F., Del Río-Hortega, J., Rafael Iglesias-Rozas, J., Garrosa, M., and Kettenmann, H. (2016). The "Big-Bang" for modern glial biology: translation and comments on Pío del Río-Hortega 1919 series of papers on microglia. Glia *64*, 1801–1840.

Sierra, A., Gottfried-Blackmore, A.C., McEwen, B.S., and Bulloch, K. (2007). Microglia derived from aging mice exhibit an altered inflammatory profile. Glia *55*, 412–424.

Sperling, R., Mormino, E., and Johnson, K. (2014). The evolution of preclinical Alzheimer's disease: implications for prevention trials. Neuron *84*, 608–622.

Suryamohan, K., and Halfon, M.S. (2015). Identifying transcriptional cis-regulatory modules in animal genomes. Wiley Interdiscip. Rev. Dev. Biol. *4*, 59–84.

Tay, T.L., Sagar, Dautzenberg, J., Grün, D., and Prinz, M. (2018). Unique microglia recovery population revealed by single-cell RNAseq following neurodegeneration. Acta Neuropathol. Commun. *6*, 87.

Thion, M.S., Low, D., Silvin, A., Chen, J., Grisel, P., Schulte-Schrepping, J., Blecher, R., Ulas, T., Squarzoni, P., Hoeffel, G., et al. (2018). Microbiome influences prenatal and adult microglia in a sex-specific Manner. Cell *172*, 500–516.e16.

Treutlein, B., Brownfield, D.G., Wu, A.R., Neff, N.F., Mantalas, G.L., Espinoza, F.H., Desai, T.J., Krasnow, M.A., and Quake, S.R. (2014). Reconstructing lineage hierarchies of the distal lung epithelium using single-cell RNA-seq. Nature *509*, 371–375.

Ungvari, Z., Krasnikov, B.F., Csiszar, A., Labinskyy, N., Mukhopadhyay, P., Pacher, P., Cooper, A.J.L., Podlutskaya, N., Austad, S.N., and Podlutsky, A. (2008). Testing hypotheses of aging in long-lived mice of the genus Peromyscus: association between longevity and mitochondrial stress resistance, ROS detoxification pathways, and DNA repair efficiency. Age (Dordr) *30*, 121–133.

Vellas, B., Sampaio, C., Bateman, R., Boxer, A., Carrillo, M.C., Cummings, J., Dubois, B., Hampel, H., Katz, R., Khachaturian, Z., et al. (2014). EU./U.S. CTAD task force on Alzheimer's trial populations. J. Prev. Alzheimers Dis. *1*, 110–116.

Verbeek, J., Vlassis, N., and Krose, B. (2002). Procrustes analysis to coordinate mixtures of probabilistic principal component analyzers. IAS-UVA-02 (Technical Report), p. 18, inria-00321503.

von Kobbe, C. (2018). Cellular senescence: a view throughout organismal life. Cell. Mol. Life Sci. *75*, 3553–3567.

Xu, W., Hiếu, T., Malarkannan, S., and Wang, L. (2018). The structure, expression, and multifaceted role of immune-checkpoint protein VISTA as a critical regulator of anti-tumor immunity, autoimmunity, and inflammation. Cell. Mol. Immunol. *15*, 438–446.

Yona, S., Kim, K.-W., Wolf, Y., Mildner, A., Varol, D., Breker, M., Strauss-Ayali, D., Viukov, S., Guilliams, M., Misharin, A., et al. (2013). Fate mapping reveals origins and dynamics of monocytes and tissue macrophages under homeostasis. Immunity *38*, 79–91.

Zeisel, A., Muñoz-Manchado, A.B., Codeluppi, S., Lönnerberg, P., La Manno, G., Juréus, A., Marques, S., Munguba, H., He, L., Betsholtz, C., et al. (2015). Brain structure. Cell types in the mouse cortex and hippocampus revealed by single-cell RNA-seq. Science *347*, 1138–1142.

STAR★METHODS

KEY RESOURCES TABLE

REAGENT or RESOURCE	SOURCE	IDENTIFIER
Antibodies		
CD45-PE, non-human primate	Miltenyi Biotec	Cat# 250204; RRID: AB_244325
Mouse anti-chicken CD45 APC	Southern Biotech	Cat# 8270-11; RRID: AB_2796475
Mouse anti-pig CD45 FITC	Bio-Rad	Cat# MCA1222F; RRID: AB_2174249
anti-human CD45	BioLegend	Cat# 304008; RRID: AB_2566370
Marmoset CD45 PE	BioLegend	Cat# 250204; RRID: AB_2562120
Anti-mouse/human CD11b	eBioscences	Cat# 17-0112-83; RRID: AB_469344
Goat polyclonal CD11b antibody	Abcam	Cat# Ab62817; RRID: AB_955740
Iba-1	Wako	Cat# 019-19741; RRID: AB_839504
Anti-leech Iba1	Jacopo Vizioli	Drago et al., 2014
anti-GFP	Invitrogen	Cat# A11122; RRID: AB_221569
anti-mCherry	Abcam	Cat# ab125096; RRID: AB_11133266
Alexa Fluor 568	Life technologies	Cat# A11011; RRID: AB_143157
anti-P2Y12	AnaSpec	Cat# AS-55043; RRID: AB_2267540
anti-Pu.1	Cell Signaling	Cat# 2258S; RRID: AB_2186909
anti-Pu.1	Abcam	Cat# ab209983; RRID: AB_10636661
Hu FcR Binding blocker	eBiosciences	Cat# 14-9161-73; RRID: AB_468582
Mouse FcR blocking antibody	BD Biosciences	Cat# 553141; RRID: AB_394656
Chemicals, Peptides, and Recombinant Proteins		
Zombie Fixable Viability Kit	BioLegend	423101
Percoll	Sigma	P1644
1xPBS	Sigma	D8537
10xPBS	GIBCO	70013065
HBSS	GIBCO	14170112
HEPES	GIBCO	15630056
Glucose 45%	Sigma	G8769
Critical Commercial Assays		
Dynabeads mRNA DIRECT Purification Kit	Invitrogen	Cat# 61012
NextSeq 500/550 High Output v2 kit (75 cycles)	Illumina	Cat# FC-404-2005
Deposited Data		
Lavin et al., 2014	GSE63341	DOI.10.1016/j.cell.2014.11.018
Raw data files for single cell RNA seq	NCBI GEO	GEO: GSE134707
Experimental Models: Organisms/Strains		
C57BL/6NCrl	Charles River- Germany	MGI:2683688
BALB/cAnNCrl	Charles River- Germany	MGI:2668903
Crl:CD1(ICR)	Charles River- Germany	MGI:5649524
FVB	Charles River- Germany	MGI:2163709
Wild Mouse /France	Diethart Tautz: Max-Planck-Institute Plön	*Mus musculus*
Goldhamster	Janvier Laboratory- Germany	RjHan:AURA
Zebrafish mpeg1:EGFP	Francesca Peri, EMBL Heidelberg	*Danio Rerio*
Macaque	Christine Stadelmann, Neuropathology, Göttingen	*Callithrix jacchus,*
Domesticated sheep	Stephan Meckel, Neuroradiology, Uniklinikum Freiburg	*Ovis Aries*

(*Continued on next page*)

Continued

REAGENT or RESOURCE	SOURCE	IDENTIFIER
Chicken CSF1R-mApple	Adam Balic, The Roslin Institute, University of Edinburgh	*Gallus gallus*
Leopard Gecko	Pet shop	*Eublepharis macularius*
Corn snake	Pet shop	*Panterophis guttatus*
Fin whale	Lífvísindasetur Læknagarðs, Iceland	*Balaenoptera physalus*
Black flying fox	Florent Ginhoux, A*STAR Singapore	*Pteropus alecto*
Axolotl	Pet shop	*Ambystoma mexicanum*
Medicinal leech	Jacopo Vizioli, University Lille	*Hirudo medicinalis*
Hermann's tortoise	Kaspar Matiasek	*Testudo hermanni*
Bearded dragon	Kaspar Matiasek	*Pogona vitticeps*
Wild pig	local hunter	*Sus scrofa*
WISTAR rat	ENVIGO	*Rattus norvegicus*
Blind mole rat	Tali Kimchi	*Spalax ehrenbergi*
Software and Algorithms		
MATLAB R2017b	MathWorks	https://www.mathworks.com/
R 3.5.0	The R Foundation	http://www.r-project.org/
Hisat 0.1.6	Kim et al., 2015	http://www.ccb.jhu.edu/software/hisat/index.shtml
GENE-E version 3.0.215	Copyright 2013 Broad Institute, Inc.	https://software.broadinstitute.org/GENE-E/
FlowJo software	FlowJo, LLC	https://www.flowjo.com
IMARIS software	Bitplane	https://imaris.oxinst.com
Other		
MARS-seq reagents	Keren-Shaul et al., 2019	https://doi.org/10.1038/s41596-019-0164-4

LEAD CONTACT AND MATERIALS AVAILABILITY

Further information and requests for reagents should be directed to and will be fulfilled by lead author Ido Amit (ido.amit@weizmann.ac.il).

This study did not generate new unique reagents.

EXPERIMENTAL MODEL AND SUBJECT DETAILS

Experimental animals

All experimental procedures were either approved by a local ethical review committee and conducted in accordance with personal and project licenses under the UK Animals (Scientific Procedures) Act (1986) or performed in accordance with institutional animal welfare guidelines and were approved by the government of Baden-Wurttemberg, Germany. Full sample information (strain, source, growth conditions, age and sex) can be found in Table S1.

Human samples

Human brain tissue was collected from healthy brain regions of individuals that underwent epilepsy surgery. The specific area of collection, as well as full sample information (source, age and sex) is documented in Table S1. All experiments were conducted in accordance with the institutional review board of the University of Freiburg Medical Center.

METHOD DETAILS

Sample processing

Mice, rats, BMR and hamsters were trans-cardially perfused with PBS before tissue extraction whereas other animals were not perfused due to size limitation. Whole brains (zebrafish, chicken, hamster, mice, rats, BMR, marmoset and macaque), or specific parts of the brain (cortex and white matter from sheep and human), were collected. For human samples, in epilepsy surgery, excess human tissue surrounding an epileptic focal was collected into ice-cold PBS immediately after resection. Absence of pathology in the sample was confirmed by histological analysis in the respective area by a neuropathologist. In post mortem sample collection, samples were included in the study only if no indication of a tumor or inflammatory disease was examined by histological analysis.

Sample processing for histology and FACS

Single-cell suspensions of tissues for all animals were achieved using mechanical dissociation followed by density gradient separation; Pellet was mixed with 37% percoll (Cat. no. P1644, Sigma) and centrifuged in 800G for 30 min at 4°C. Supernatant was discarded and pellet was taken further for antibody staining, as described below. Cell suspension was treated with 1:4000 diluted DAPI solution in 1xPBS to label dead cells. Before proceeding with antibody staining, cells were pre-incubated with mouse or human Fc receptor blocking antibody (BD Biosciences, Cat. 553141) for 20 minutes at 4°C. For antibody staining, cells were incubated with antibody cocktail for 20 minutes at 4°C. For FACS staining and setups, cells were acquired on FACS Canto, LSRII and LSR Fortessa systems (BD Biosciences) and analyzed using Flowjo software (TreeStar).

Histology

Histology was performed as described (Erny et al., 2015). Brains were removed and fixed in 4% buffered formalin. Then brain tissue was dehydrated and embedded in paraffin. 3 μm thin sections were stained with Iba1 (cat. no. 019-19741, Wako) for all species except leech-specific Iba1 (Drago et al., 2014; provided by J.V.), anti-GFP (cat. no. A11122, Invitrogen) for zebrafish and anti-mCherry (cat. no. ab125096, Abcam) for chicken microglia. In addition, brain tissue was stained for P2Y12 (cat. no. AS-55043, AnaSpec) or with anti-GFP (cat. no. A11122, Invitrogen) for zebrafish as well for PU.1 (Cat. no. 2258S, Cell Signaling, zebrafish: cat. no. ab209983, Abcam) At least 3–4 brain sections per sample were evaluated.

Flowcytometry single cell sorting

Cell populations were sorted using MoFlo Astrios (Beckman Coulter). Prior to sorting, all samples were filtered through a 70-μm nylon mesh (Cat. no. 352350, Corning). Samples were gated for $CD45^+$ after exclusion of doublets and dead cells. Isolated cells were single cell sorted into 384-well cell capture plates containing 2 μl of lysis solution and barcoded poly(T) reverse-transcription (RT) primers for scRNA-seq (Keren-Shaul et al., 2019). Immediately after sorting, each plate was spun down to ensure cell immersion into the lysis solution, snap frozen on dry ice, and stored at –80°C until processed.

Flowcytometry bulk cell sorting

Cell populations were sorted using MoFlo Astrios (Beckman Coulter). Prior to sorting, all samples were filtered through a 70-μm nylon mesh (Cat. no. 352350, Corning). Samples were gated for $CD11b^+CD45^{lo}$ microglia population or GFP^+ cells for zebrafish or $CD45^+CSF1RmApple^+$ cells for chicken, after exclusion of doublets. 10,000 cells were sorted into a low-bind Eppendorf tube containing 40 μl of lysis binding buffer (Invitrogen). Immediately after sorting, tubes were spun down to ensure cell immersion into the lysis solution, snap frozen on dry ice, and stored at –80°C until processed.

Flowcytometry antibody table

Name	Source	Catalogue #	Secondary
CD45-PE, non-human primate	Miltenyi Biotec	130-091-897	
Mouse anti-chicken Bu-1a/b	Bio-Rad	MCA5764	IgG1
Mouse anti-sheep CD45	Bio-Rad	MCA896GA	IgG1
Mouse anti-chicken CD45 APC	Southern Biotech	8270-11	
Mouse anti-pig CD45 FITC	Bio-Rad	MCA1222F	
Marmoset CD45 PE	BioLegend	250204	
Alexa Fluor 488	BioLegend	406416	Anti-IgG
Mouse anti-human CD45 PE	BioLegend	304058	
Anti-mouse CD11b	eBioscences	17-0112-83	
Mouse FcR blocking antibody	BD Biosciences	553141	
Hu FcR Binding blocker	eBiosciences	14-9161-73	
Anti-NHP CD45 PE	BD Biosciences	552833	
Anti-Rat CD45 PE	BD Biosciences	554888	
Goat polyclonal CD11b antibody	Abcam	Ab62817	Goat IgG
Donkey anti-Goat IgG (H+L) APC	R&D systems	F0108	Anti-goat IgG

Massively Parallel Single-Cell RNA-seq Library preparation (MARS-seq2.0)

Single-cell libraries were prepared as previously described (Keren-Shaul et al., 2019). In brief, mRNA from cell sorted into cell capture plates are barcoded and converted into cDNA and pooled using an automated pipeline. The pooled sample is then linearly amplified by T7 *in vitro* transcription, and the resulting RNA is fragmented and converted into a sequencing-ready library by tagging the

samples with pool barcodes and Illumina sequences during ligation, RT, and PCR. Each pool of cells was tested for library quality and concentration is assessed as described earlier (Keren-Shaul et al., 2019).

Bulk RNA-seq library preparation

10,000 cells from each population were sorted into 40 μl of lysis/binding buffer (Invitrogen). mRNA was captured with 12 μl of Dynabeads oligo(dT) (Invitrogen), washed, and eluted at 85°C with 10 μl of 10 mM Tris-Cl (pH 7.5). We used a derivation of MARS-seq as described (Keren-Shaul et al., 2019), developed for scRNA-seq to produce expression libraries with a minimum of three replicates per population. See details in Table S1.

QUANTIFICATION AND STATISTICAL ANALYSIS

Three-dimensional reconstruction of microglia

Reconstruction of microglial cells was performed as previously described (Erny et al., 2015). 30-μm parasagittal FFPE sections from adult brain tissue were stained with anti-Iba1 (cat. no. 019-19741, Wako) for all species except leech-specific Iba1 (Drago et al., 2014; provided by J.V.), anti-GFP (cat. no. A11122, Invitrogen) for zebrafish and anti-mCherry (cat. no. ab125096, Abcam) for chicken microglia for 48 hr, respectively (dilution 1:500 at 4°C), followed by Alexa Fluor 568–conjugated secondary antibody (cat. no. A11011, Life technologies) staining, which was added at a dilution of 1:500 overnight at 4°C. Nuclei were counterstained with DAPI. Imaging was performed on an Olympus Fluoview 1000 confocal laser scanning microscope (Olympus) using a 20 × 0.95 NA objective. Z stacks were done with 1.14-μm steps in z direction, 1,024 × 1,024 pixel resolution were recorded and analyzed using IMARIS software (Bitplane). At least three cortical cells were reconstructed per analyzed sample.

Bulk low-level processing and filtering

Mapping of reads was done using HISAT (version 0.1.6) (Kim et al., 2015). Reads sharing a Unique Molecular Identifier (UMI) sequence mapped to the same genome region (< 3kb distance) were considered as one UMI. Reads were associated with genes if they were mapped to an exon in the correct orientation of the gene. Gene expression tables were created using analyzeRepeats.pl script from the HOMER package (v4.8) giving the species specific GTF file (-gff flag) and genome from Ensembl as input (http://homer.ucsd.edu/homer/).

Ortholog gene selection

To compare transcription between species, we first created a gene ortholog table using the mouse genome as the reference gene list. We performed gene homology search, using ensemble multiple species comparison tool (http://www.ensembl.org/biomart/martview/42ddd77f8b0f4aae7d9eefe32cc4518c). Each species was compared to mouse and a high-quality ortholog genes list was extracted (gene order conservation score above 75, whole genome alignment score above 75 and minimum sequence identity above 80%). To account for gene paralogs and gene-duplication events, an aggregated table of ''meta-genes'' was created. Each meta-gene may include all gene symbols homologous to one mouse gene. For each organism, read counts were combined across all manifestations of each meta-gene. For example, if zebrafish's actb1 had two reads, and actb2 three reads, the actb meta-gene received a total of five reads. Missing genes in species were given an ''A'' value.

Deconvolution of bulk data by detecting single cell outliers

Bulk RNA-seq data can contain a mixture of cell types due to sample acquisition impurity and existence of outlier and/or ''contaminating'' cells. Therefore, scRNA-seq data was used to deconvolute bulk samples with the following approach. First, single-cell data from each organism was clustered using the Metacell package (see below; Baran et al., 2018) and clusters were manually annotated as either microglia or ''contaminating'' cell types, based on expression of core genes shared by all species. Each bulk sample was treated as a linear combination of all the cell types included in the scRNA-seq data. Using the optimization algorithm ''L-BFGS-B'' in R general-purpose function ''optim,'' we computed the contribution of the contaminating Metacells. Then, we deconvoluted each bulk RNA-seq sample by subtracting the relative contribution of the contaminating clusters.

Bulk RNA-seq normalization

Comparing bulk RNA-seq data between species is especially challenging due to differences in the total number of genes, total read number, housekeeping genes expression profiles, and possible other factors that affect conventional RNA-seq normalization methods. To overcome this technical challenge, we used gene-rank scores instead of actual read count methods (such as TPM/RPKM). Each meta-gene in every bulk sample was scored based on its UMI count rank in that sample (scores ranged between 0 and 1). The resulting scores vector was used as the transcription profile for all downstream analysis. Rank scores were floored to 0.5. To discard lowly expressed genes, only genes with at least one entry ranked higher than 0.8 were included in later analysis. Overall, ~9k genes were used for downstream clustering and analysis (Figure 3A).

Bulk RNA-seq clustering

Ranked bulk RNA-seq data were clustered using the K-means algorithm (MATLAB R2018a function K-means). The value of k was chosen by assessing the mean silhouette values (a measure of how close each point in one cluster is to points in the neighboring clusters) for various k parameters and selecting k that maximizes the average silhouette.

Gene enrichment analysis

We performed gene enrichment analysis of the human specific cluster and the large mammalian cluster (cluster 11 and 12 of Figure 3A) using the online software Metascape (http://metascape.org/) tool with default parameters, setting all genes as background. Genes from human senescent-like microglia cell cluster has been removed from the analysis. To test for enrichment for genes related to neurodegenerative diseases, we used GWAS gene lists from the NHGRI-EBI GWAS catalog (mapped to Genome Assembly GRCh38.p12 and dbSNP Build 151) and perform hypergeometric distribution test for each cluster from Figure 3A. $p < 0.01$ was considered significant.

Single cells RNA-seq low-level processing and filtering

All single cell RNA-seq libraries were sequenced using Illumina NextSeq 500 at a median sequencing depth of: human 39032, mouse 47777, zebrafish 31764, chicken 63187, marmoset 57111, macaque 43212, sheep 47170, hamster 55582, rat 18633, Blind mole rat 11679 reads per single cell. For detailed statistics in single cell resolution on barcodes, reads, mapping and genes see Table S1. Sequences were mapped to appropriate genome, demultiplexed, and filtered as previously described (Jaitin et al., 2014; Keren-Shaul et al., 2019), extracting a set of UMIs that define distinct transcripts in single cells for further processing. We estimated the level of spurious UMIs in the data using statistics on empty MARS-seq wells as previously described (Jaitin et al., 2014). Mapping of reads was done using HISAT (version 0.1.6) (Kim et al., 2015); reads with multiple mapping positions were excluded. Reads were associated with genes if they mapped to an exon, using the appropriate ensemble v90 reference genome. Exons of different genes that shared genomic position on the same strand were considered a single gene with a concatenated gene symbol.

Single cells data processing and clustering

The Metacell pipeline (Baran et al., 2018) was used to derive informative genes and compute cell-to-cell similarity, to compute a K-nn graph cover and derive a distribution of RNA in cohesive groups of cells (or Metacells), and to derive strongly separated clusters using bootstrap analysis and computation of graph covers on resampled data. Default parameters were used unless otherwise stated. Cells with high (> 32 UMI) expression of hemoglobin genes were discarded (e.g., Hbb, Hba1, Hba2). ERCC genes were discarded. Mitochondrial genes and ribosomal genes were removed from the list of features used for the Metacell analysis. Cells with less than 500 total UMI were discarded as low-quality cells. We used bootstrapping to derive robust clustering (500 iterations; resampling 70% of the cells in each iteration, and clustering of the co-cluster matrix with minimal cluster size set to 20). No further filtering or cluster splitting was performed on the Metacells.

Single cell RNA-seq differential expression analysis

To compare single cell expression between species, UMI tables were transformed to meta-genes as described above. For each organism, we used Metacell analysis to discard outlier cells. Each cell was normalized by cell size and log transformed. We tested for significantly differential genes by FDR adjusted Wilcoxon test (p value $< 10^{-10}$ and fold change > 2).

Pooling single cell RNA-seq data

In order to compare single cell RNA-seq data to the deconvoluted bulk clustering in Figure 3A (Figure S4A), we collected single cells from microglia associated Metacells and computed the pooled expression for each species. The expression vector for each species was then rank-ordered as was done for the bulk data. Cluster assignments were derived from the K-means clustering performed on the bulk RNA-seq data.

Scatterplots

To generate scatterplots in Figures S4D and S4E, we used spearman correlation of log-transformed UMI-counts of single cell RNA-seq described in the previous section. All genes from microglia core gene module (Figure 3A) were plotted unless an orthologous gene did not exist in one of the two compared species.

PCA

PCA in Figure S4 was performed in MATLAB R2018a (function PPCA) (Verbeek et al., 2002) based on sensible principal components analysis.

Defining a module gene signature

To define a module gene signature for Metacells 3-6 of the human microglia (Figure 4F), we used the normalized UMI table to identify the most differential genes between our clusters and identified a group of 26 genes (e.g., *Cdkn1*, *Ccl2*, *Tnf*) that exhibited a strong Pearson correlation across the Metacells' log2 footprint expression of the 200 most variable genes excluding genes associated with

mitochondria and stress that were filtered from these lists in advance. The *p-value* was calculated using Wilcoxon signed-rank test and false discovery rate (FDR) correction. The threshold for differential genes was set at *p*Value < 1E-7.

DATA AND CODE AVAILABILITY

The accession number for gene expression analysis in the paper is available at NCBI GEO: GSE134707. Scripts reproducing the analysis are available at: https://bitbucket.org/amitlab/.

Genomes

	Species	Built	Ensemble
Human	*Homo sapiens*	hg38	ensemble v95
Mouse	*Mus musculus*	mm10	ensemble v95
Chicken	*Gallus gallus*	galGal5	ensemble v90
Marmoset	*Callithrix jacchus*	calJac3	ensemble v90
Macaque	*Macaca fascicularis*	Mmul 8.0.1	ensemble v90
Sheep	*Ovis aries*	Oar v3.1	ensemble v90
Zebrafish	*Danio rerio*	danRer10	ensemble v90
Hamster	*Mesocricetus auratus*	MesAur1.0	ensemble v90
Rat	*Rattus norvegicus*	Rnor 6.0	ensemble v95
Blind Mole Rat	*Nannospalax galili*	S.galili v1.0	ensemble v96

ADDITIONAL RESOURCES

We have generated a web-based tool to provide easy data exploration access of all gene expression datasets generated in this study: https://amitlab.shinyapps.io/Orthologous_viewer/.

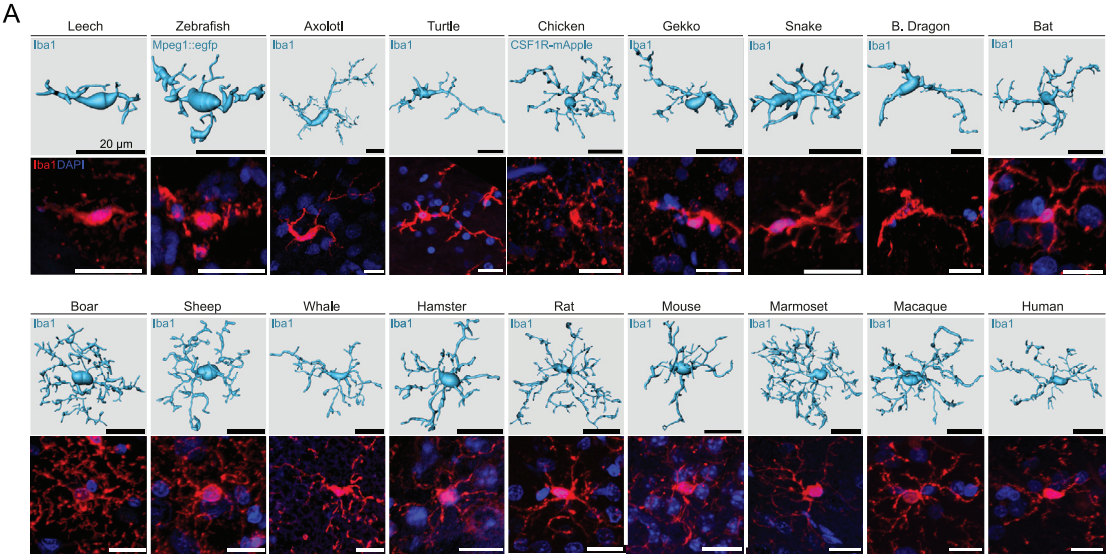

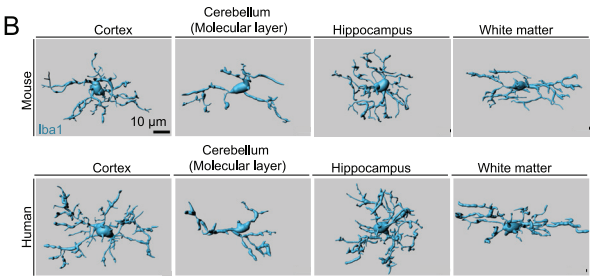

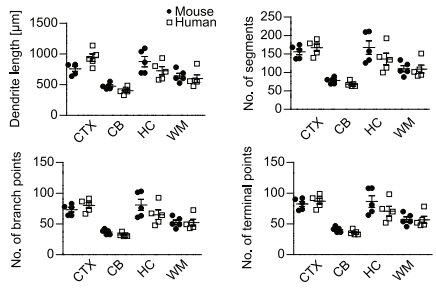

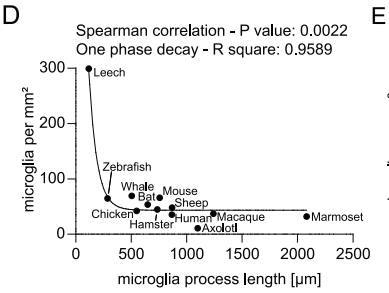

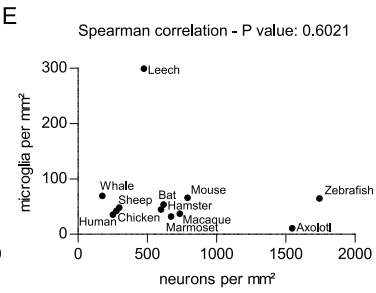

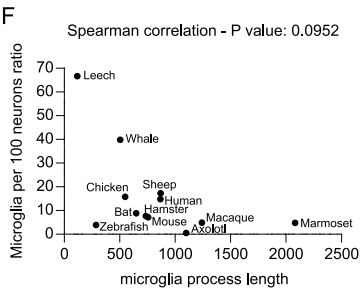

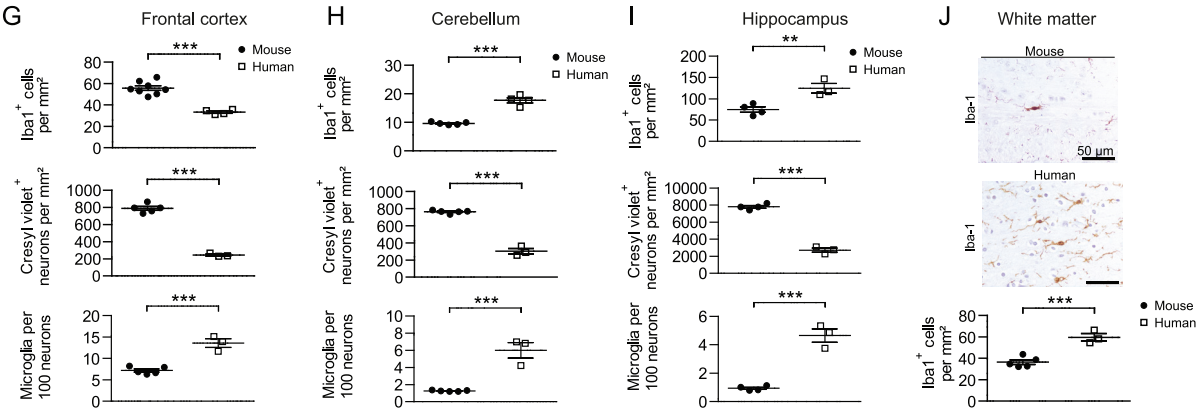

(legend on next page)

Figure S1. Quantitative Analysis of Microglia Morphology in Evolutionarily Distant Animals, Related to Figure 1

(A) Representative reconstructed ramified parenchymal microglia cells and corresponding fluorescence images of Iba1$^+$, Mpeg1-eGFP$^+$ (zebrafish) and CSF1R-mApple$^+$ (chicken) microglia (red) and DAPI (4′,6-diamidino-2-phenylindole, blue) from all analyzed species. Scale bar represents 20 μm. (B) Three-dimensional reconstruction (scale bar represents 10 μm) of cortical mouse and human Iba1$^+$ microglia from different brain regions (cortex, cerebellum, hippocampus and white matter). Each symbol displays one individual sample with at least three measured cells per species. Data is presented as mean ± SEM (C) Imaris-based automatic quantification based on data from panel (B) of dendrite length, number of segments, branch points and terminal points of microglia from different brain regions (cortex (CTX), cerebellum (CB), hippocampus (HC) and white matter (WM)). Each symbol displays one individual sample with at least three measured cells per species. (D)-(E) Spearman correlation analysis comparing microglia per mm^2 and microglia process length (D), microglia per mm^2 and neurons per mm^2 (E) and microglia per 100 neurons ratio and microglia process length (F). (G-J) Quantitative assessment of mouse and human microglia and neurons in different brain regions. Iba1$^+$ microglia and cresyl violet$^+$ neurons in the mouse and human frontal cortex (G), cerebellum (H), hippocampus (I) and white matter; on top a representative image (J). Scale bar represent 50 μm. Each symbol displays one individual sample. Data is presented as mean ± SEM. Significant differences were determined by an unpaired t test and marked with asterisks (**$p < 0.01$, ***$p < 0.001$).

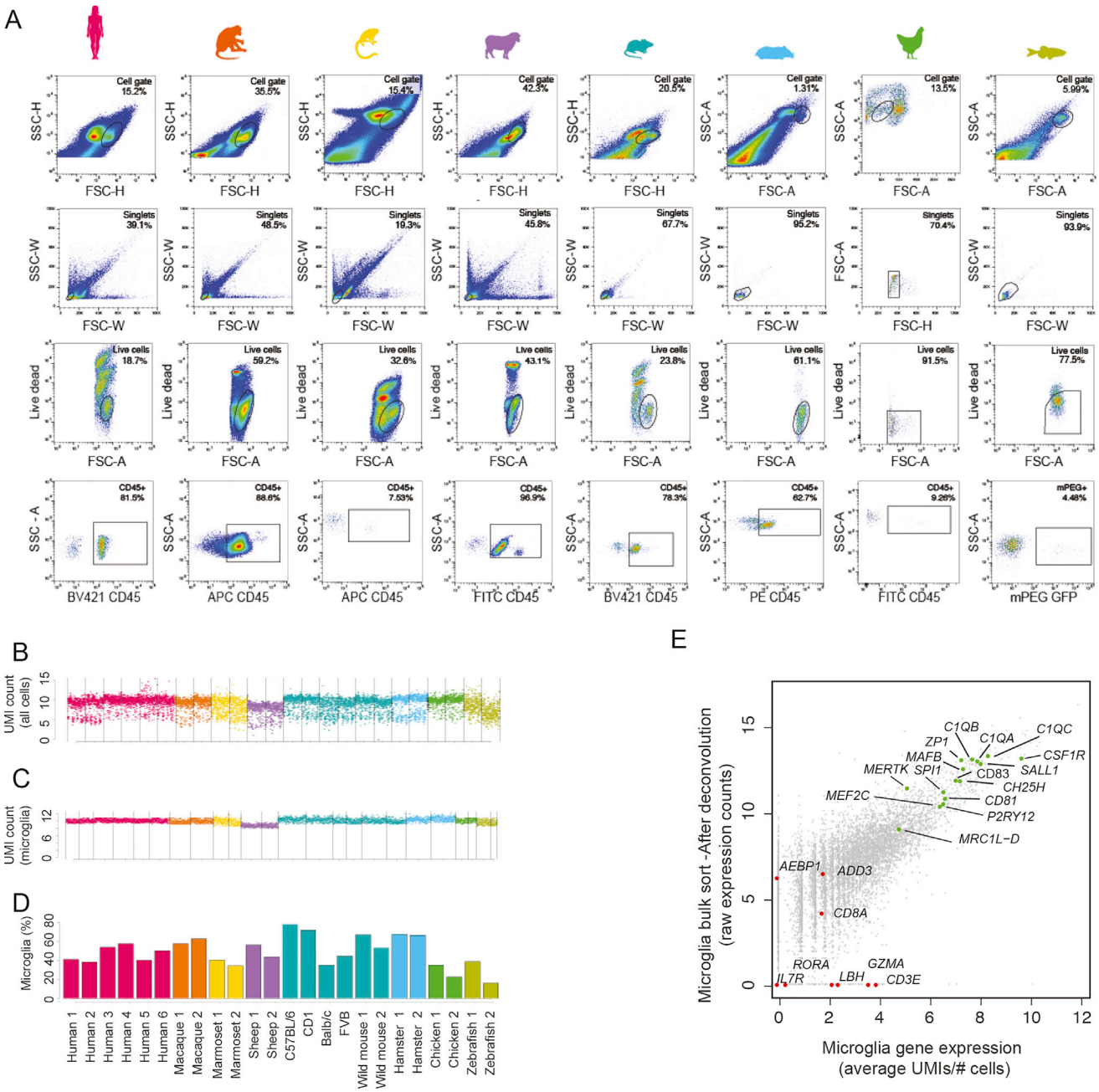

Figure S2. Cross-Species Microglia Isolation, Related to Figure 2

(A) Representative flow cytometry plots showing gating strategy for brain CD45$^+$ scRNA-seq sort. (B) Total UMI/cell count per sample/animal. (C) UMI/cell count after filtering for microglia. (D) Percentage of microglia identified in each species from flow cytometry sorted brain CD45$^+$ single cells. (E) Scatter (xy) plot showing the relationship of expressed genes between single cell RNA-seq of chicken microglia based on Figure 2B cluster (x) and bulk RNA-seq of chicken microglia after deconvolution (y).

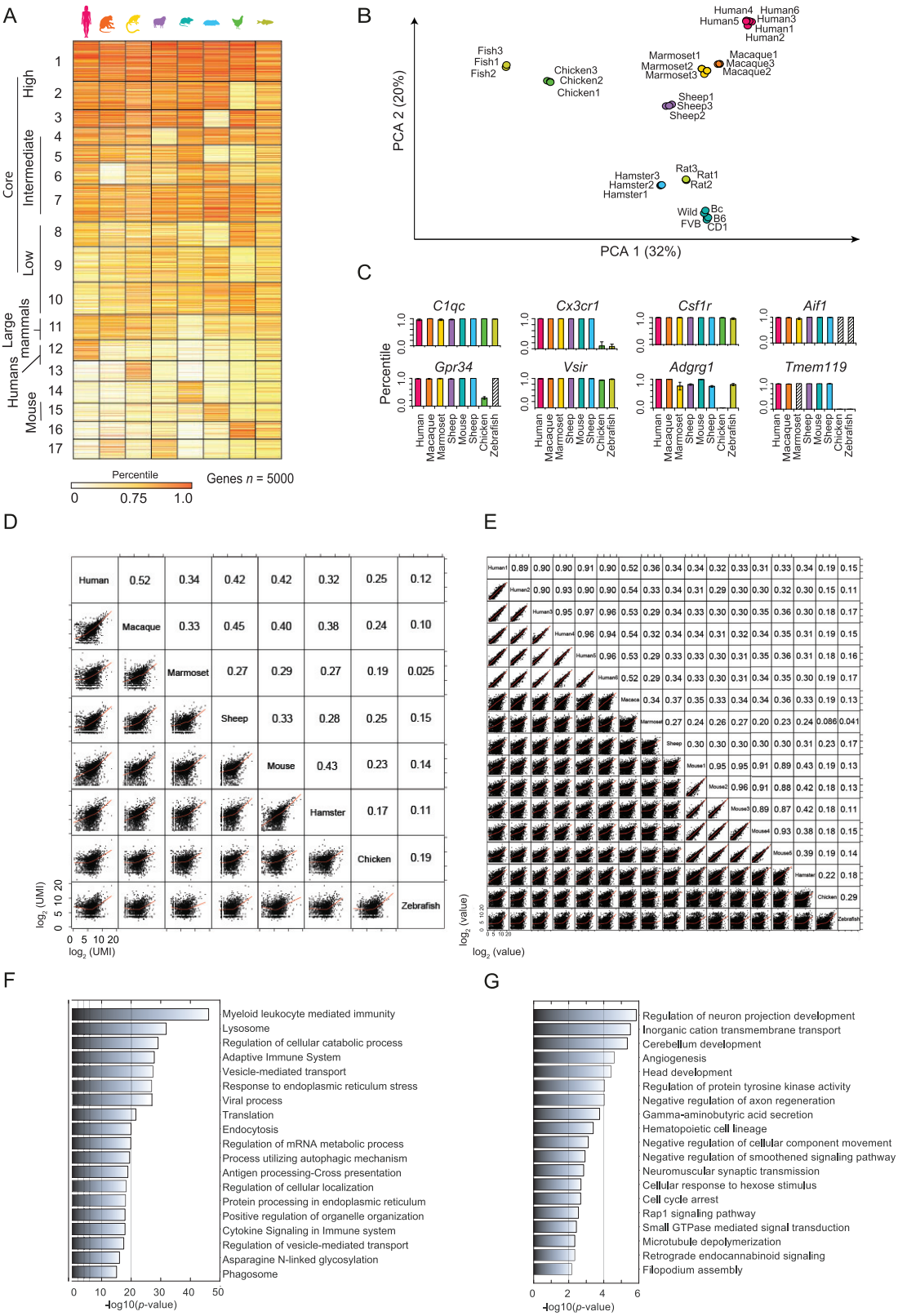

(legend on next page)

Figure S3. Analysis of the Microglia Gene Program across Evolution, Related to Figure 3

(A) Heatmap representation of an average of scRNA-seq expression (UMIs per cell/number of cells) of microglia across species (row). Clustering of most differentiated genes (k = 17). (B) Principal component analysis (PCA) plot of all genes from all species and their biological replicates. (C) Bar plots of ranked bulk RNA-seq expression of representative highly conserved and highly expressed genes identified from clusters 1-3 (as shown in Figure 3A). Error bars show standard deviation. Genes with no orthologs are marked with a diagonally striped bar. (D-E) Correlation of global expression signature of microglia across species measured by Spearman rank correlation (r_s) of the single cell RNA-seq (D) and the bulk RNA-seq (E). Significant biological processes or pathways identified using Metascape software analysis of all genes from clusters 1-3 using all genes as a background (F) or microglia specific genes identified in a comparative analysis of tissue macrophages and microglia in Figure 3D, using all genes as a background (G).

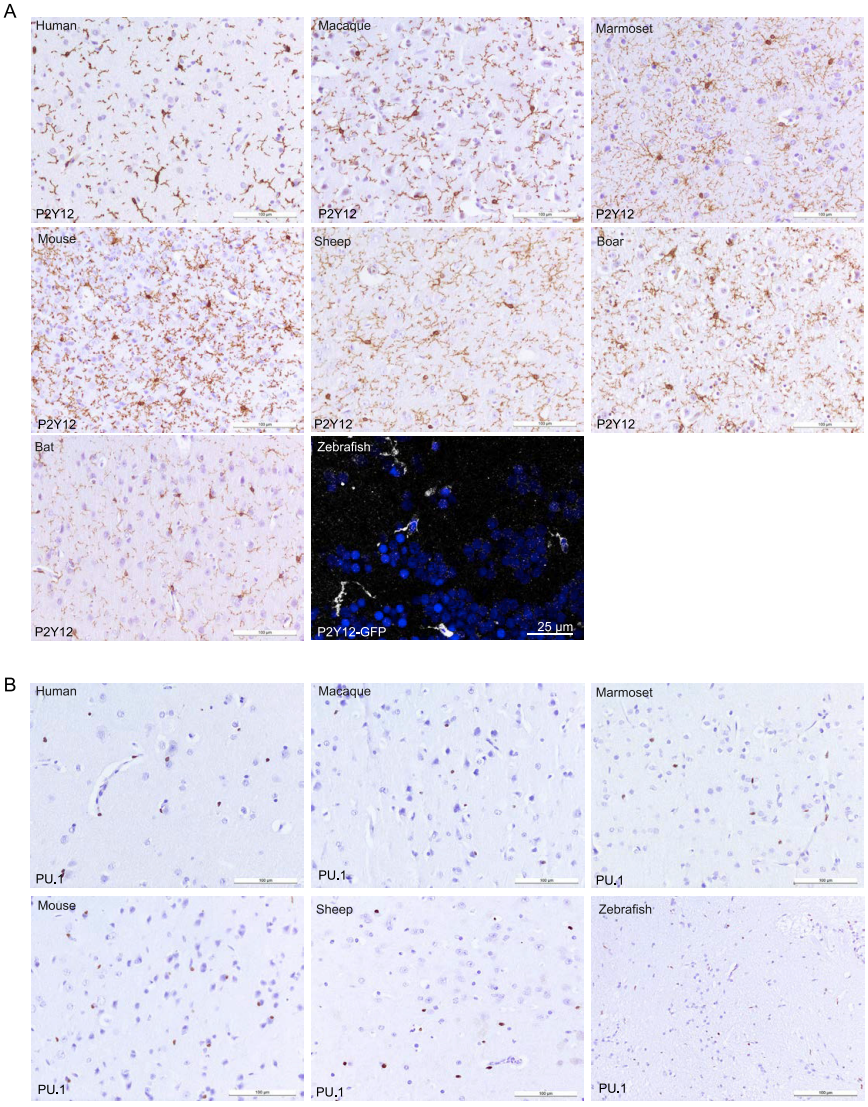

Figure S4. Conservation of P2Y12 and PU.1 across Microglia Evolution, Related to Figure 3

(A) Representative P2Y12 immunohistochemistry microscopical images from paraffin brain sections from human, macaque, marmoset, mouse, sheep, boar or bat as well as representative immunofluorescence image from brain section from zebrafish. Scale bar represents 100 μm or 25 μm (zebrafish). (B) Representative PU.1 immunohistochemistry microscopical images from paraffin brain sections from human, macaque, marmoset, mouse, sheep or zebrafish. Scale bars represents 100 μm.

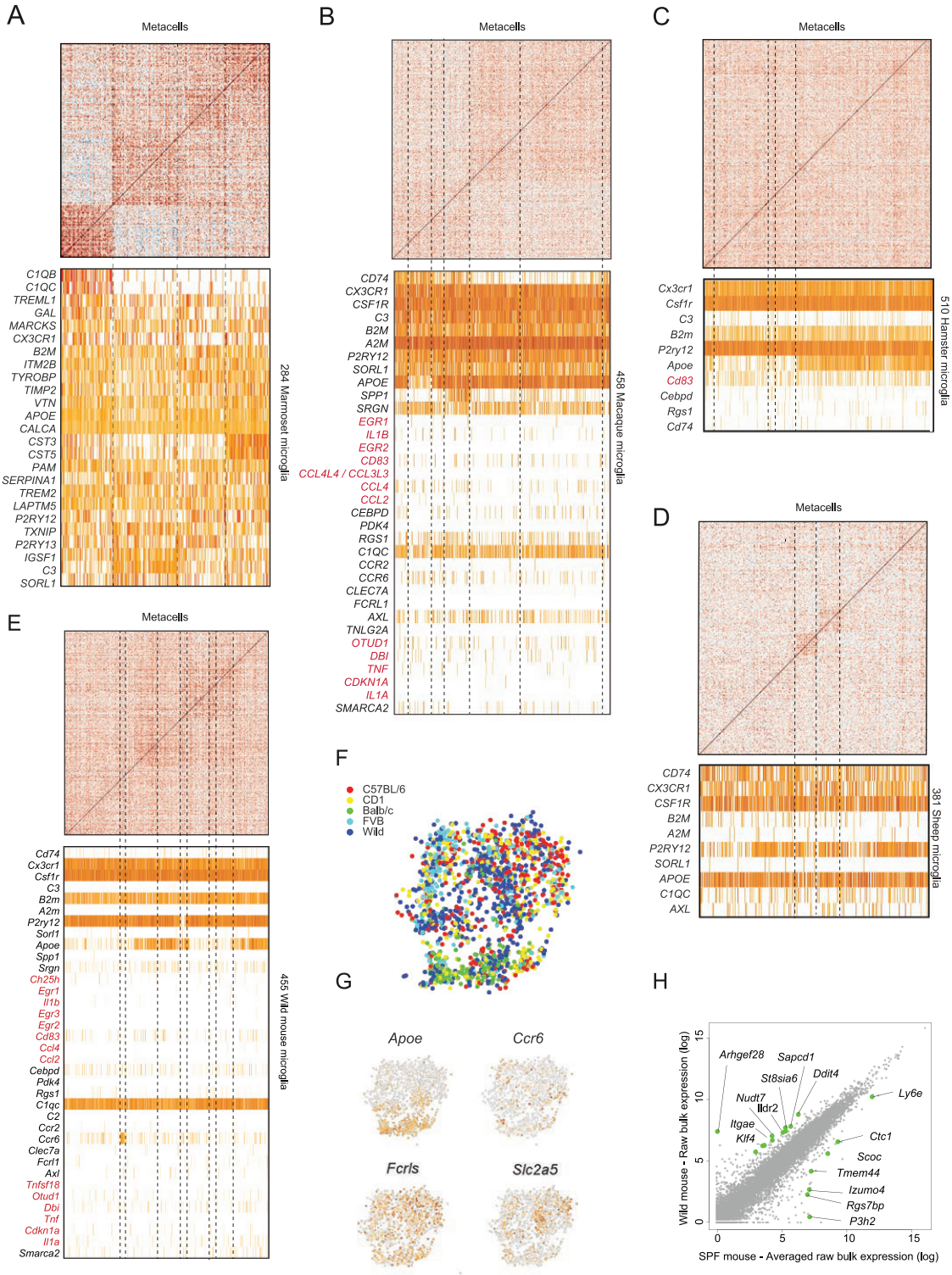

Figure S5. Microglia Transcriptional Heterogeneity within Species, Related to Figure 4

(A-E) Cell-to-cell correlation plots of microglia and corresponding heatmaps for most differentially expressed genes. In the heatmaps, each mark represents one cell and each row the cells from one individual. (A) Marmoset microglia (5 pooled brains). (B) Macaque microglia (5 pooled brains). (C) Hamster microglia (5 pooled

(legend continued on next page)

brains). (D) Sheep microglia (5 pooled brains). (E) Wild mouse microglia (4 pooled brains). (F) A tSNE plot showing five mouse strains: C57BL/6, BALB/c, CD1, FVB (5 pooled brains each strain) and Wild mice (4 pooled brains). (G) A tSNE plot of the most differentiated marker genes expressed in mouse strains. The intensity of color corresponds to increased expression. (H) An x-y plot comparing bulk RNA-seq of wild mouse microglia with averaged bulk RNA-seq expression of mouse strains in SPF conditions (C57BL/6, CD1, BALB/c, FVB). The most significant genes (Wild versus SPF averaged) are labeled.

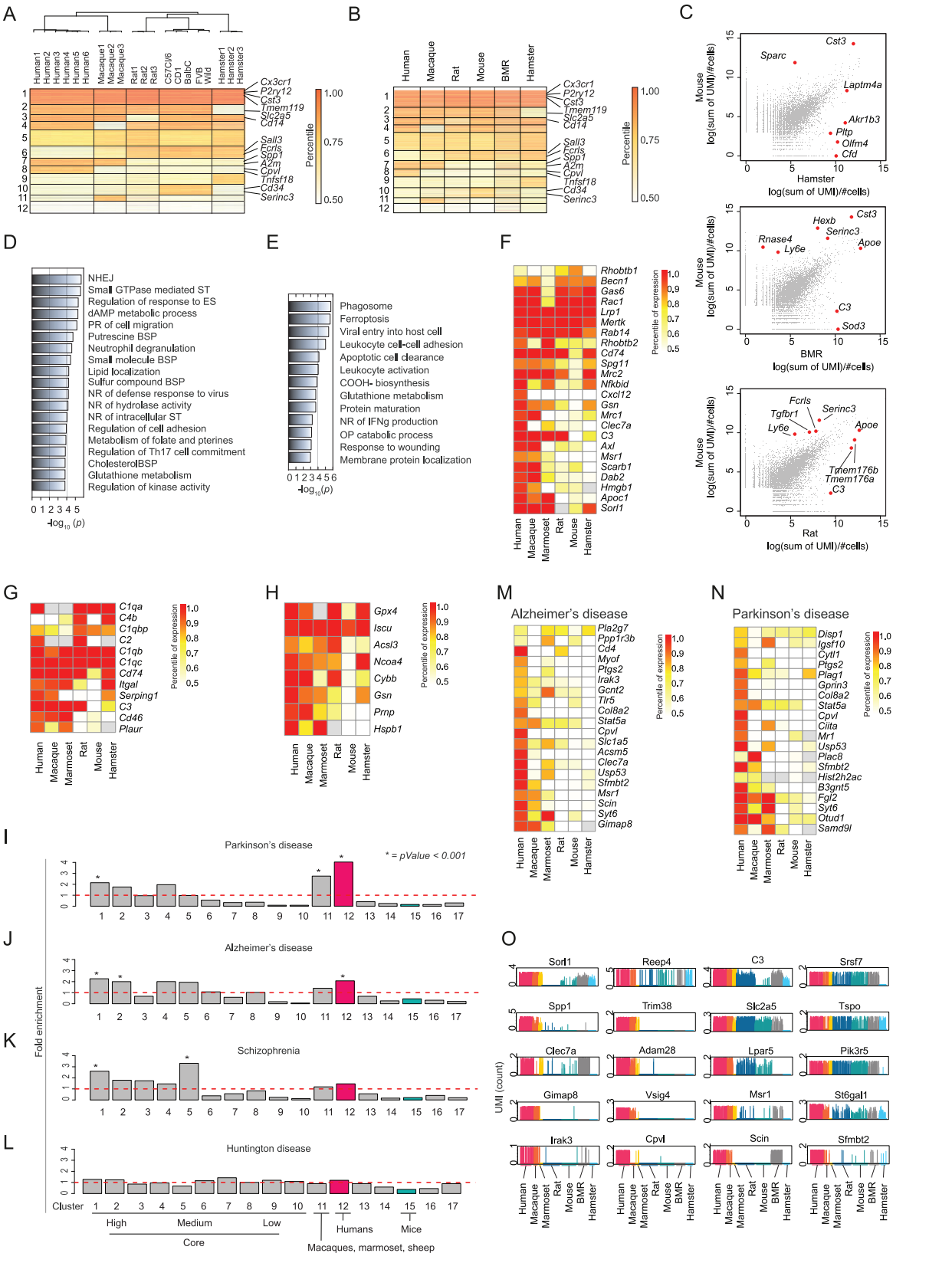

(legend on next page)

Figure S6. Characterization of Microglia Species-Specific and Disease-Associated Pathways, Related to Figure 5

(A-B) Heatmap representation and clustering of most differentiated genes (k = 12) of (A) a deconvoluted bulk of microglia and (B) an average of scRNA-seq expression (UMIs per cell/number of cells) of microglia across species (row). (C) x-y plots comparing bulked single cell RNA-seq of rodents to each other. Highest differentially expressed genes are demonstrated. (D) Gene ontology (GO) terms enriched in human, macaque, marmoset and sheep microglia (cluster 11; Figure 3A). Differential genes from human senescent-like microglia has been removed from the analysis. Abbreviations: Non-homologous end-joining (NHEJ), signal transduction (ST), external stimulus (ES), deoxyribonucleoside monophosphate (dAMP), biosynthetic process (BSP), negative regulation (NR), positive regulation (PR), T helper 17 (Th17). (E) Gene ontology (GO) terms enriched in homeostatic human microglia (cluster 8; A). Differential genes from human senescent-like microglia were removed from the analysis. Abbreviations: Monocarboxylic acid (COOH-), negative regulation (NR), interferon gamma (IFNg), organophosphate (OP) (F-H) Heatmap representations of Gene ontology (GO) terms enriched in clusters related to (A). Genes from human senescent microglia cell cluster were removed from the analysis. Highest significantly enriched pathways in homeostatic human microglia (cluster 8) are represented. (F) Specific genes from the classical complement pathway (GO: 0006956). (G) Specific genes from apoptotic cell clearance (GO: 0043277). (H) Specific genes from ferroptosis pathway (GO: 0097). Grey boxes indicate non-ortholog. (I-L) Clusters identified from cross-species comparison of microglia (from Figure 3A) and visual demonstration of enrichment of GWAS terms shown as fold change per cluster for Parkinson's disease (I), Alzheimer's disease (J), Schizophrenia (K) and Huntington disease (L). Hypergeometric test was used to calculate the statistical significance of under- or over-representation of a module of genes in clusters. Significantly enriched GWAS gene lists (p = 0.001) are marked with an asterisk (*). Human clusters are colored in pink; mouse clusters are colored in light blue. (M-N) Heatmap of gene expression of specific susceptibility genes for AD (M) or PD (N) defined by published GWAS from the NHGRI-EBI GWAS catalog (mapped to Genome Assembly GRCh38.p12 and dbSNP Build 151). Genes that are specifically absent or lowly expressed in mouse but not in humans are demonstrated. Grey boxes indicate there is no homologous gene. (O) A sparkline plot of specific genes related to specific neurodegenerative diseases defined by published GWAS as in panels M and N.